International Immunopharmacology 123 (2023) 110725

Contents lists available at ScienceDirect

International Immunopharmacology

journal homepage: www.elsevier.com/locate/intimp

Immunoinformatics-based multi-epitope vaccine design for the re-emerging monkeypox virus

Mahour Farzan [a,b,1], Mahan Farzan [a,b,1], Yousef Mirzaei [c], Sara Aiman [d], Fatemeh Azadegan-Dehkordi [e,*], Nader Bagheri [f,**]

[a] Medical Plants Research Center, Basic Health Sciences Institute, Shahrekord University of Medical Sciences, Shahrekord, Iran
[b] Student Research Committee, Shahrekord University of Medical Sciences, Shahrekord, Iran
[c] Department of Medical Biochemical Analysis, Cihan University-Erbil, Kurdistan Region, Iraq
[d] Faculty of Environmental and Life Sciences, Beijing University of Technology, Beijing 100124, China
[e] Cellular and Molecular Research Center, Basic Health Sciences Institute, Shahrekord University of Medical Sciences, Shahrekord, Iran
[f] Clinical Biochemistry Research Center, Basic Health Sciences Institute, Shahrekord University of Medical Sciences, Shahrekord, Iran

ARTICLE INFO

Keywords:
Multi-epitope vaccine
Monkeypox virus (MPXV)
Molecular docking
Molecular dynamics
Immunoinformatics

ABSTRACT

Background: On May 7, 2022, WHO reported a new monkeypox case. By May 2023 over 80,000 cases had been reported worldwide outside previously endemic nations. (This primarily affected the men who have sex with men (MSM) community in rich nations). The present research aims to develop a multi-epitope vaccine for the monkeypox virus (MPXV) using structural and cell surface proteins.

Methods: The first part of the research involved retrieving protein sequences. The Immune Epitope Database (IEDB) was then used to analyze the B and T lymphocyte epitopes. After analyzing the sensitizing properties, toxicity, antigenicity, and molecular binding, appropriate linkers were utilized to connect selected epitopes to adjuvants, and the structure of the vaccine was formulated. Algorithms from the field of immunoinformatics predicted the secondary and tertiary structures of vaccines. The physical, chemical, and structural properties were refined and validated to achieve maximum stability. Molecular docking and molecular dynamic simulations were subsequently employed to assess the vaccine's efficacy. Afterward, the ability of the vaccine to interact with toll-like receptors 3 and 4 (TLR3 and TLR4) was evaluated. Finally, the optimized sequence was then introduced into the Escherichia coli (*E. coli*) PET30A + vector.

Results: An immunoinformatics evaluation suggested that such a vaccine might be safe revealed that this vaccine is safe, hydrophilic, temperature- and condition-stable, and can stimulate innate immunity by binding to TLR3 and TLR4.

Conclusion: Our findings suggest that the first step in MPXV pathogenesis is structural and cell surface epitopes. In this study, the most effective and promising epitopes were selected and designed through precision servers. Furthermore, through the utilization of multi-epitope structures and a combination of two established adjuvants, this research has the potential to be a landmark in developing an antiviral vaccine against MPXV. However, additional in vitro and in vivo tests are required to confirm these results.

1. Introduction

Newly recognized diseases have recently undergone epidemiological shifts, increasing incidences in various parts of the world [1,2]. These Emerging infectious diseases (EIDs) place a heavy financial strain on society and result in numerous public health complications [1,2]. EIDs can develop when previously harmless pathogens acquire new virulence factors or when infections spread to previously unaffected regions [1,2]. While the world is still grappling with the aftermath of the COVID-19 pandemic, the emergence of the monkeypox virus (MPXV) as an infectious disease seems problematic [3].

Human monkeypox (MPX) is a zoonotic disease caused by the large

* Corresponding author.
** Corresponding author.
E-mail addresses: fatemehazadegan@gmail.com (F. Azadegan-Dehkordi), n.bagheri1985@gmail.com (N. Bagheri).
[1] These two authors considered both as first author of this work (Mahour Farzan, Mahan Farzan).

https://doi.org/10.1016/j.intimp.2023.110725
Received 17 January 2023; Received in revised form 25 July 2023; Accepted 26 July 2023
Available online 7 August 2023

double-stranded DNA genome of the monkeypox virus [4]. MPXV is comparable to smallpox but less severe clinically [4]. MPXV symptoms (including fatigue, headache, fever, and myalgia) typically last two to three weeks [4]. In some sensitive populations, such as children, pregnant women, and people with certain medical conditions (immunodeficiency diseases and immunosuppressed patients), the progression of MPXV infection can vary [5]. Nevertheless, close contact with an infected person is typically considered a risk factor [5].

The mortality rate from MPXV is high, ranging from 1% to 11% [6]. Smallpox was eradicated due to a worldwide vaccination campaign organized by the World Health Organization (WHO), which saved millions of lives. Therefore, most countries stopped vaccinating against this virus after WHO eradicated smallpox in 1980 [7]. After nearly 40 years, the world's population still lacks effective protection against smallpox and only partially protects against other poxviruses (such as monkeypox) induced by smallpox vaccines [8]. There has been a resurgence of MPXV due to newly reported cases of infection. Therefore, this virus was designated as an emerging disease in 2018 by the World Health Organization Research and Development (WHO R&D) Blueprint [9].

Although the world has not fully overcome the COVID-19 pandemic and its repercussions, the increasing number of human MPXV-positive cases in several non-endemic regions is cause for significant concern [7]. As a result of the devastating effects of previous pandemics (such as the COVID-19 pandemic) on the global health system and societies, we must prevent another raging EID from becoming a devastating pandemic [10].

Vaccination is an effective method for preventing EIDs like MPX. Several vaccines that induce immunization against MPXV have been developed; however, these vaccines are not designed specifically for MPXV and have low efficacy. Vaccines designed specifically against MPXV are still undergoing preliminary testing [11]. In addition, according to a report by the Centers for Disease Control and Prevention (CDC), no specific therapeutic method exists for MPXV [5]. Consequently, new treatment methods, including vaccination, are required to combat emerging MPXV strains.

The immune system plays an important role in pathogenesis and the fight against viruses and cancer [12]. Vaccines must induce an immune response faster than the pathogen to be effective. Nevertheless, conventionally designed vaccines like Dryvax and Jynneos are expensive, time-consuming, allergenic, and have production safety concerns

Table 1
Multi-epitope vaccines against MPXV.

Docking	Adjuvant	Number of Amino acids	Selected genes/proteins	Study
TLR-2 TLR-3 TLR-4	Beta-defensin 3	Monkey pox vaccine- 1 306	A21L, A30L, A43R, B8R, B9R, B20R, C22L, J2R	[107]
	50S ribosomal protein L7/L12	Monkey pox vaccine- 2 388		
	Heparin binding hemagglutinin	Monkey pox vaccine- 3 417		
TLR-4	HBHA protein	Monkey pox vaccine- 1 511	B5R, J3L, F8L, B17R, I8R, B5R, C1L, B1R, C2L, J6R, D3R, E8L, C19L, A25R, B4R, B12R, A48R, B14R, A46R, A40L, R1R, C4L, D18L, F3L	[5]
	Beta defensin	Monkey pox vaccine- 2 397		
	HBHA conserved peptide	Monkey pox vaccine- 3 502		
	50S ribosomal protein L7/L12	Monkey pox vaccine- 4 482		
TLR-2 TLR-3	Human beta-defensin 2	N/A	L1R, B5R, A33R	[16]
TLR-2 TLR-4 TLR-8	Cholera-toxin B subunit	180	Cupin domain-containing protein ABC transporter ATP-binding protein DUF192 domain-containing protein	[17]
TLR-9	50S ribosomal protein	308	NP_536428.1, AAQ09810, AAM76335.1, AAM76334.1, URF91554.1, USS79525.1	[18]
TLR5	Flagellin protein and RS09	390	AIE40790.1, AIE40786.1, AIE40780.1, AIE40778.1, AIE40774.1, AIE40766.1, AIE40764.1, AIE40763.1, AIE40759.1, AIE40758.1, AIE40739.1, AIE40738.1, AIE40737.1, AIE40733.1, AIE40718.1, AIE40702.1, AIE40669.1, AIE40657.1	[19]
TLR2	50S ribosomal protein L7/L12	377	MPXVgp181	[20]
TLR3	50S ribosomal L7/L12	Monkey pox V1 494 Monkey pox V2 366	COP-B7R COP-A44L	[21]
TLR4	CTxB	167	MV-6, MV-12, MV-13, MV-20, MV-28, MV-42, MV-147, MV-150, MV-158, MV-170	[22]
TLR3 TLR4	Cholera toxin b (CTB)	150	E8L	[106]
TLR4	HBHA HBHA conserved B -defensin L7/L12 ribosomal proteins (MPXV-V4)	Monkey pox V4 326	L5L, A28, L5	[13]
MHC I alleles (HLA-A*02:01, HLA-B*15:01), and MHC class II allele (HLA-DRB1)	RS09 and PADRE	275	E8L	[11]
TLR4	CTxB	376	cell surface-binding protein envelope protein A28 homolog	[13,14]
TLR2 TLR4	CTB	207	Aligned sequences of different MPXV strains	[15]
TLR3 TLR4	β-defensin-3, protein LL-37	749	A27L, A29L, B14R, E13L, A34L	Our study

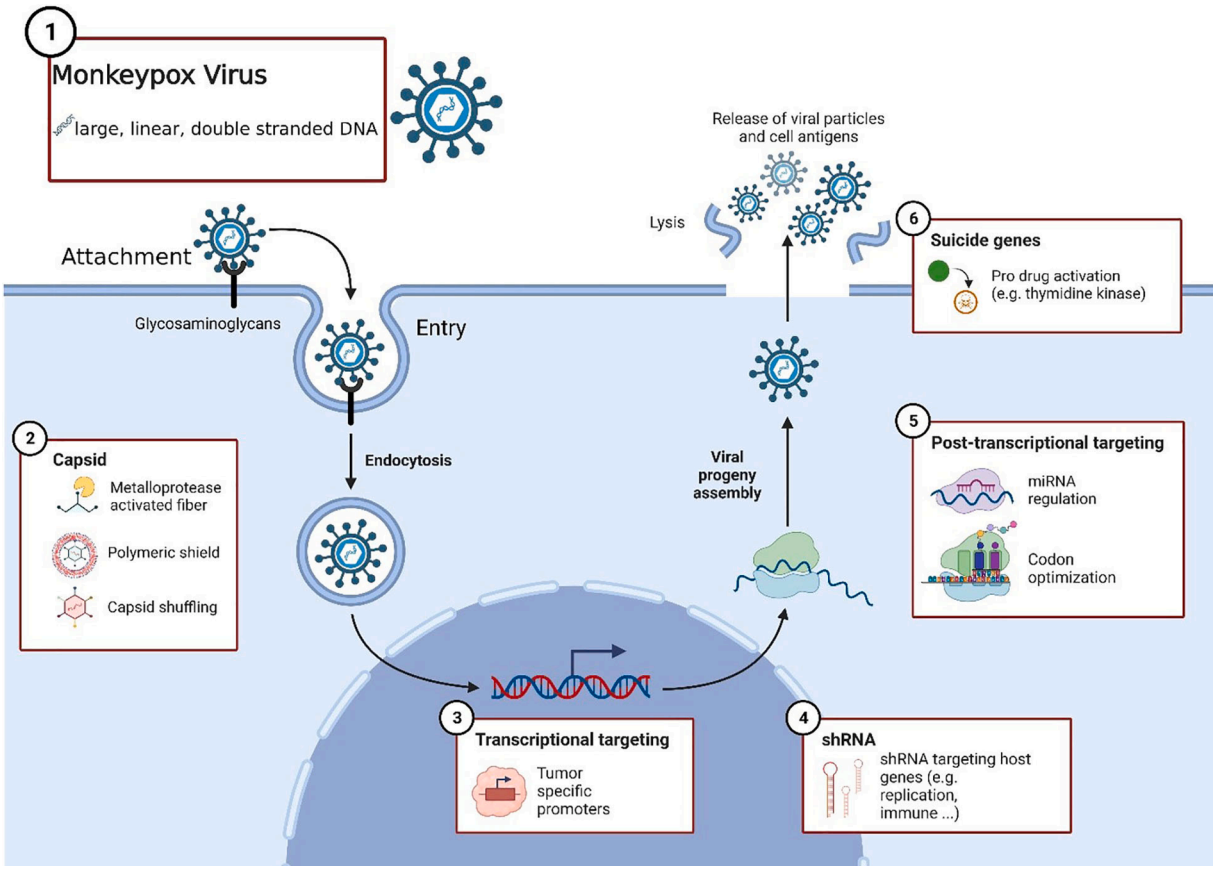

Fig. 1. Schematic overview of the monkeypox virus life cycle.

[11]. A fundamental component of humoral and cellular immune responses is an epitope. Recent advances in immunoinformatics have allowed us to design multi-epitope vaccines that are extremely safe and cost-effective [13]. Table 1 summarizes the designed multi-epitope MPXV vaccines [13–22]. The A27L gene encodes a protein (A-type inclusion body protein) that is associated with the intracellular mature virus (IMV) and plays a crucial role in the host immune response [23]. This protein is believed to play a role in poxvirus entry [24].

There are reports that monoclonal antibodies (MAbs) specific to A27L can be immunoprotective [25,26]. In brief, the virus invades the body and multiplies in lymphocytes during the pathogenesis of MPX [24]. A29L can promote viral membrane fusion with the host plasma membrane by binding to heparin on the cell surface [24]. B14R, also known as interleukin (IL)-1B binding protein, is believed to be one of the genes responsible for the increased virulence of certain MPXV strains [27]. The scaffold protein D13 (E13L gene) gives immature virions (IV) a rigid and curved convex membrane that rifampicin targets [28]. ATPase/DNA packaging protein (A34L protein) is a structural protein of enveloped virions that performs DNA packaging into virions and is NTP-binding motif A [29]. The MPXV life cycle is schematically depicted in Fig. 1.

We developed novel vaccines against MPXV based on predicted T- and B-cell epitopes using reverse vaccinology and biophysical techniques in this study. This study aimed to examine the immunoinformatics data of A34L, A29L, B14R, E13L, and A27L proteins to identify effective and immunogenic epitopes for the design of multi-epitope recombinant proteins in light of the obstacles above and the significance of the disease. Vaccines based on these proteins' highly conserved regions can be used to protect against MPXV because they do not evolve.

2. Methodology

The systematic workflow used in this study to design a subunit multi-epitope vaccine construct against MPXV is depicted in Fig. 2.

2.1. Protein target sequence retrieval

We isolated the complete dsDNA sequence for MPXV and all proteins encoded by the virus's genome. Approximately 180 MPXV proteins were isolated and characterized. Accessing the UniProt database (https://www.uniprot.org/) in the common FASTA format (accessed on 04.2022), we were able to retrieve the full sequences of the MPXV target proteins and vaccine adjuvants, which we then verified with NCBI data entry (Table 2).

Antigenicity predictions were made using the ANTIGENpro server (https://scratch.proteomics.ics.uci.edu/) and the VaxiJen server (https://www.ddgpharmfac.net/vaxijen/VaxiJen/VaxiJen.html) for the selected protein sequences. To determine whether or not the proteins mentioned above were allergenic, we used the online tool AllerTOP2.0 (https://www.ddg pharmfac.net/AllerTOP/method.html) (Table 3). The human body's immune cells must be able to identify the viral protein sequence because this recognition triggers allergic reactions [30,31]. Select proteins' transmembrane helices were determined using TMHMM-2.0 (https://services.healthtech.dtu.dk/service.php?TMHMM-2.0). Subcellular localization was performed using the CELLO2GO web server (https://cello.life.nctu.edu.tw/cello2go/) [32,33]. The virulence factors of the selected proteins were also predicted using the VirulentPred web server [34].

2.2. Prediction and selection of 9-mer and 15-mer T-cell epitopes

Vaccine candidates were narrowed down to those proteins that could

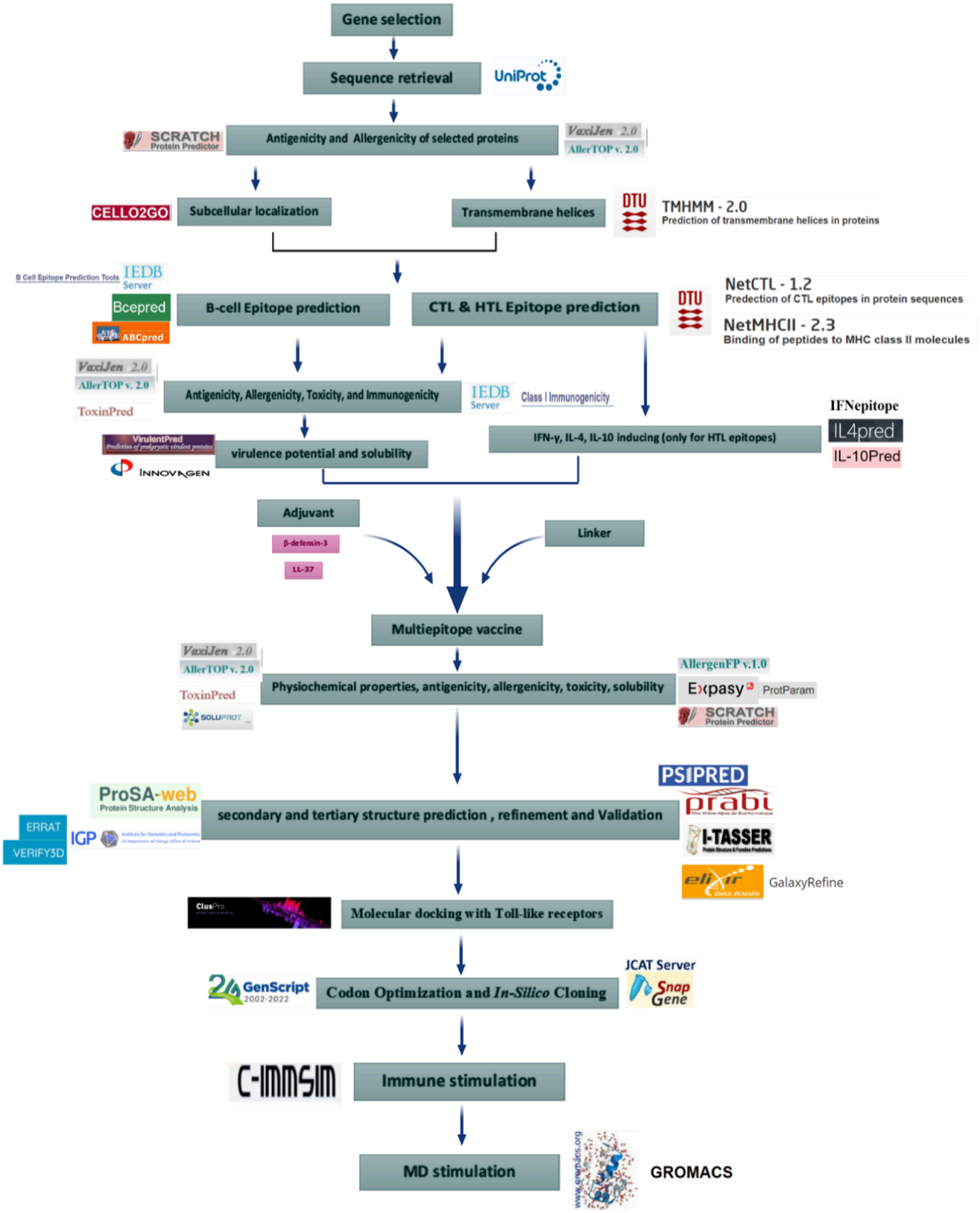

Fig. 2. The systematic workflow of this study.

Table 2
The parameters set for the C-ImmSim server.

Parameter	Value
Random Seed	12,345
Simulation Volume	30
Simulation Steps	1000 (About 1 year)
Injection N. 1 Time step of injection	1
What to inject	Vaccine (No LPS)
Injection N. 2 Time step of injection	84
What to inject	Vaccine (No LPS)
Injection N. 3 Time step of injection	170
What to inject	Vaccine (No LPS)

Table 3
The accession number of the selected proteins for vaccine design.

Accession number	Protein/Gene name	Length (Amino acids)
Q8V4V1	A-type inclusion body protein (A27L)	696
Q77HM6	IMV surface fusion protein (A29L)	110
Q8V4R4	IL-beta-binding protein (B14R)	326
Q8V4X5	Scaffold protein D13 (E13L)	551
Q8V4U5	ATPase A32 /DNA packaging protein (A34L)	300

cross the cell's outer membrane. The surface topology of the target proteins was considered during the selection of immunogenic determinants (epitopes) for the subunit vaccine. Major histocompatibility complex (MHC) molecules, such as class I and II, represent T-cell epitopes [5]. These molecules are recognized by two subsets of T-cells, CD8 and CD4, respectively. Epitopes for cytotoxic T lymphocytes (CTLs) were identified in 12 MHC class I supertypes using the NetCTL 1.2 server (https://www.cbs.dtu.dk/services/NetCTL/) [35]. The server relies on artificial neural network (ANN) predictions of MHC class I peptide binding, ANN predictions of proteasomal C-terminal cleavage, and a weight matrix-based method of calculating TAP transfer efficiency [36–38]. The C-terminal cleavage efficiency, TAP transport effectiveness, and epitope detection thresholds were set as defaults (0.15, 0.05, and 0.75, respectively).

In addition, we used the NetMHCII-2.3 server (https://services.healthtech.dtu.dk/service.php?NetMHCII-2.3) to predict the MCH class II-restricted CD4 + helper T lymphocyte (HTL) epitopes among the shortlisted proteins based on HLA-DR, HLA-DQ, and HLA-DP MHC class II alleles [39]. The thresholds for strong and weak binders were established at 2% and 10%, respectively [40,41]. MHC I alleles with an IC_{50} binding affinity of 100 nM or less, binding to more supertypes, and covering most of the population were selected for further analysis [5]. For MHC II, epitopes binding to more alleles with IC_{50} values less than 500 nM were selected for further examination [42]. Moreover, all epitopes' antigenicity, allergenicity, and toxicity were predicted. A higher antigenicity score indicates a more significant immune response. The toxicity of the predicted epitopes was evaluated using the Toxin-Pred server. Physiochemical properties of epitopes, including amphipathicity, hydrophilicity, molecular weight, pI, hydropathicity, and charge, were also calculated.

Furthermore, Virulentpred (Cascaded SVM module with a threshold of 0.0) (https://203.92.44.117/virulent/submit.html) and the Innovagen website (https://www.innovagen.com/proteomics-tools) were used to select virulent and soluble epitopes, respectively [31]; both were able to evaluate antigenic, non-allergenic, and non-toxic selected epitopes. To evaluate the immunogenicity of MHC-II epitopes, we used the MHC class I immunogenicity tool (https://tools.iedb.org/immunogenicity/)

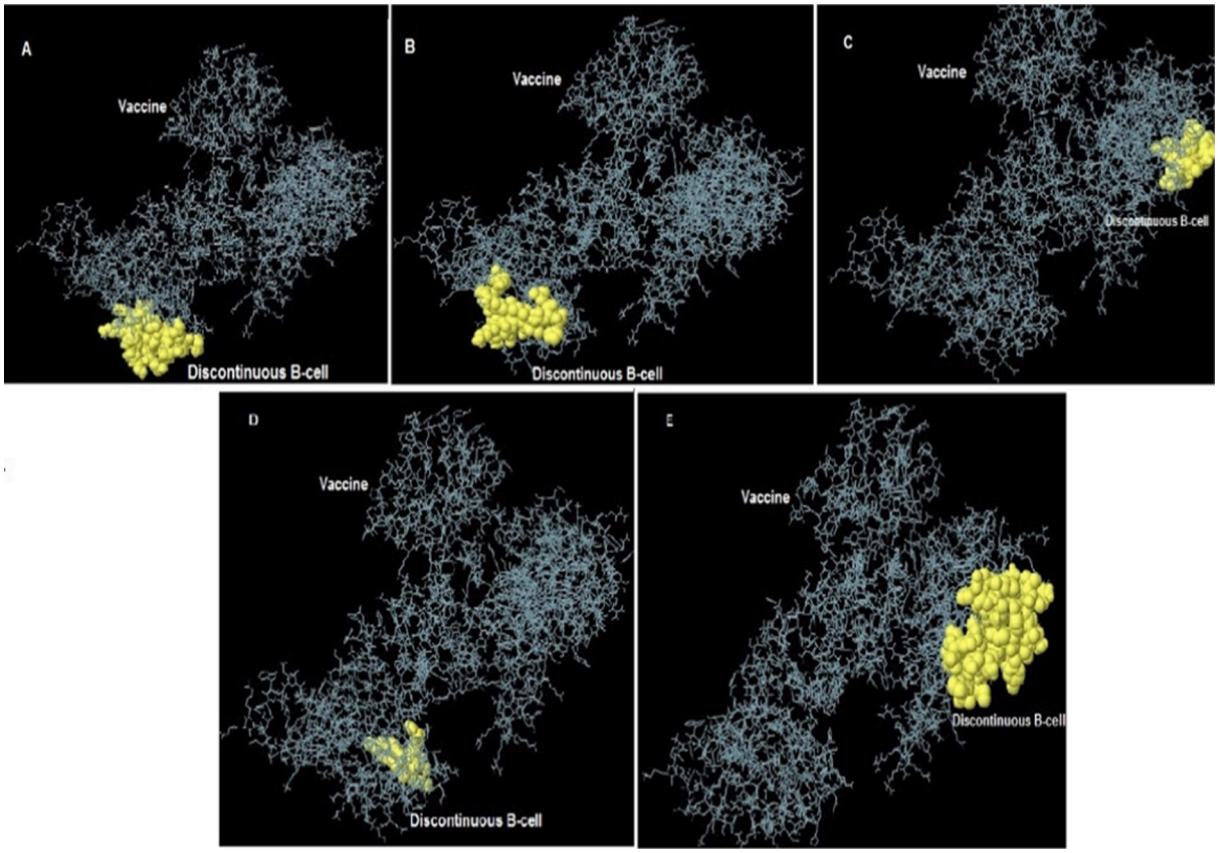

Fig. 3. The three-dimensional model shows discontinuous B-cell epitopes of 41 residues in response to vaccine (A), discontinuous B-cell epitopes of 18 residues in response to vaccine (B), discontinuous B-cell epitopes of 30 residues in reaction to vaccine (C), discontinuous B-cell epitopes of 15 residues in response to vaccine (D), discontinuous B-cell epitopes of 7 residues in response to vaccine (E).

available through the IEDB server [43].

Producing cytokines is a major feature of selected HTL epitopes in vaccine construction [44]. To this end, we analyzed the HTL epitopes for cytokine-inducing properties (Interferon-gamma (IFN-γ), Interleukin 4 (IL-4), and Interleukin 10 (IL-10)) employing IFNepitope (https://webs.iiitd.edu.in/raghava/ifnepitope/application.php), IL-4pred (https://crdd.osdd.net/raghava/il4pred/), and IL-10pred (https://webs.iiitd.edu.in/raghava/il10pred/) [45–47].

2.3. B-cell linear and discontinuous epitope prediction

B-cells are essential immune system components for the production of protective antibodies. B- cell epitopes were predicted using the ABCPred server (https://webs.iiitd.edu.in/raghava/abcpred/ABC submission.html), IEDB B-Cell Epitope Prediction Tool (https://tools.iedb.org/main/bcell/), and BCPREDS server (https://crdd.osdd.net/raghava/bcepred/). The optimal epitopes were chosen based on their high scores, and the cutoff value was established at 0.8. The discontinuous B-cell epitopes within the subunit vaccine construct were predicted using the ElliPro web server (https://tools.iedb.org/elliPro/) [48]. This server predicted epitopes with default parameters (minimum score of 0.5 and maximum score of 0.6). As the vaccine structure folds and a tertiary structure is formed, new discontinuous B-cell epitopes can be generated. Therefore, we predicted that the refined tertiary structure of the vaccine construct would contain these epitopes.

2.4. Multi-epitope vaccine construct

Subunit vaccines against MPXV were developed by combining carefully selected CTL, HTL, and B-cell epitopes with appropriate linkers and adjuvants (Fig. 3). Glycine-rich linkers (GPGPG) were used to fuse HTL epitopes to improve solubility and adjacent domain action, while alanine-rich linkers (AAY) were used to fuse CTL epitopes [49,50]. KK linkers were used to form a chain of linear B-cell epitopes [49]. Generally, linkers improve the vaccine's stability and allow each epitope to function independently after injection [5]. To improve immunogenicity and induce durable innate and adaptive immunity, the N-terminus of the subunit vaccine was fused to two potent immunostimulatory adjuvants (β-defensin-3 and antibacterial protein LL-37) via the EAAAK linker. Toll-like receptors (TLR)-1, TLR-2, and TLR-4 agonists, beta-defensin-3, contain around 40 amino acids [51]. Due to its chemotactic and modulatory activities in different immune cells, the human antimicrobial peptide LL-37 shows promising potential as a vaccine adjuvant [52]. Fig. 3 shows a schematic structure of the subunit vaccine construct.

2.5. Vaccine physiochemical properties, antigenicity, allergenicity, toxicity, and solubility evaluation

We used the ExPASy server's ProtParam tool (https://web.expasy.org/cgi-bin/protparam/protparam) to predict the physiochemical properties of the constructed subunit vaccine. These properties included the grand average of hydropathicity (GRAVY), number of amino acids, amino acid composition, molecular weight (MW), theoretical pI, half-life, instability index, and aliphatic index [53]. Various web-based tools were used to predict the modeled vaccine's antigenicity, allergenicity, and solubility [54].

2.6. Population coverage evaluation

Immune responses to pathogens in humans are highly correlated with the host's immunogenetic constitution. Variants in genes involved in the immune response can influence susceptibility to infection and set the stage for either a favorable or unfavorable immunopathologic outcome [55–57]. Polymorphisms in HLA-encoding genes have been found to have the strongest correlations with both infection outcomes and the efficacy of vaccines [56,57]. Since HLA variants have been found in numerous populations across the globe, it is now imperative that HLA variant distribution analysis be incorporated into the vaccine development process. To predict the distribution of certain MHC-I and MHC-II epitopes (HLA-I/II alleles) across the world's population, we used the IEDB population coverage tool (https://tools.immuneepitope.org/population/) [58]. The HLA allele frequencies of 78 populations across 16 regions are available on this server.

2.7. Vaccine construct secondary and tertiary structure prediction

We used the PSIPRED server (http:// bioinf.cs.ucl.ac.ukpsipred/) to construct the secondary structures of the vaccine [59]. PSIPRED evaluates the PSI-BLAST output using two feed-forward neural networks to provide simple and accurate 2D homology modeling [60]. The secondary structural patterns of the peptides were determined via SOPMA (https://npsa-prabi.ibcp.fr/cgi-bin/npsaautomat.plpage=/NPSA/npsasopma.html) [61]. Subsequently, the Prabi server was utilized to predict the proportion of secondary structural elements in the multi-epitope vaccine (https://npsa-prabi.ibcp.fr/cgi-bin/npsa automat.pl?page=/NPSA/npsa gor4.html). Through GOR IV, the server predicted an accuracy of 64.4% [62]. The I-TASSER server (https://zhanggroup.org/I-TASSER/) enables the prediction of high-quality tertiary structure models from amino acid sequences.

The confidence score (C-score) (range: −5 to 2) was employed to evaluate the predictive model's quality [63]. A model with a higher C-score is estimated to be more reliable than one with a lower C-score. The protein's structure was predicted using the (PS) 2 server (https://ps2.life.nctu.edu.tw/). The Galaxy refined server (https://zhanggroup.org/ModRefiner/) was utilized to refine the model prediction [64]. Afterward, the refined 3D model was validated via Ramachandran plot analysis, different quality factors, and error plot analysis via the PDBsum server (https://www.ebi.ac.uk/thorntonsrv/databases/pdbsum/Generate.html) [65].

ProSA-web (serverhttps://prosa.services.came.sbg.ac.at/prosa.php) shows Z-scores, X-ray, NMR, and local quality plots relative to the overall model quality. In addition, ERRAT (https://servicesn.mbi.ucla.edu/ERRAT) was used to determine non-bonded interactions between atoms in protein structures [66]. Estimates of the agreement between the tertiary structure and the amino acid sequence were computed through Verify 3D (https://www.doe-mbi.ucla.edu/verify3d/) [67]. Additionally, the vaccine construct was validated using PROCHECK (https://saves.mbi.ucla.edu/). PROCHECK generates Ramachandran plots, which display the percentages of the most favored, allowed, and prohibited amino acids [68].

2.8. Vaccine molecular docking with TLRs

We used molecular docking, a type of bioinformatics modeling, to evaluate the interaction between two or more molecules/sequences. This method relies on the three-dimensional structure of any complex and the binding properties of the ligand and target. Therefore, we evaluated the binding affinity of the designed vaccine and immune receptors (TLR3; PDB ID: 1ZIW and TLR4; PDB ID: 4g8a) by employing molecular docking approaches with the ClusPro v2 server (https://cluspro.bu.edu/login.php) [69,70]. ClusPro was utilized to calculate the center-weighted score [71,72]. Docked complexes with high binding affinities were subjected to molecular docking simulations. TLRs play a significant role in the virus detection and activation pathways of potent and prompt innate immune systems. Consequently, they may be promising vaccine development targets [73].

2.9. Molecular dynamic (MD) simulation

Molecular dynamics (MD) simulations were used to evaluate the TLR-vaccine structures derived from docking simulations. GROMACS 4.6.5 was utilized to determine the structural stability of the vaccine-

Table 4
Predicted Antigenicity and allergenicity of the selected proteins sequences.

Protein	Vaxijen score	Antigenicity (VAXIJEN)	Antigenicity (ANTIGENpro)	Antigen pro score	Allergenicity	Virulence based on amino acid sequence	Transmembrane helices count
A27L	0.3371	Non-Antigen	Antigen	0.850592	Non-allergen	Virulent (1.0079)	1
A29L	0.3128	Non-Antigen	Antigen	0.621101	Non-allergen	Virulent (0.3392)	0
B14R	0.5796	Antigen	Antigen	0.771612	Non-allergen	Virulent (0.9820)	0
E13L	0.5269	Antigen	Antigen	0.763067	Non-allergen	Virulent (0.9927)	0
A34L	0.3589	Non-Antigen	Antigen	0.696202	Non-allergen	Virulent (1.0766)	2

receptor complex. The complexes were positioned in the center of a box and filled with water using the tip3 water model. For neutralization, random water molecules were substituted with ions. The systems were simulated using NPT and NVT ensembles under periodic boundary conditions. A pressure of 1 bar was set under isotropic conditions using the Parrinello-Rahman algorithm. PME [74] was used to compute electrostatic interactions, and the LINCS procedure [75] was utilized to constrain all hydrogen-atom bonds.

The essential dynamics method constructs a covariance matrix to observe protein coordinate fluctuations. MD trajectories demonstrate correlations between motions found in the eigenvectors of the non-mass covariance matrix [76,77]. After neutralization, the steepest descent algorithm was employed for energy minimization. 100 ps of MD equilibration was performed with positional restraints on protein-heavy atoms with a spring constant of 1000 kcal.mol^{-1}nm^{-2} to prevent non-physical conformational changes in the solvated protein. The final MD simulation ran for 100 ns without restriction.

The root-mean-square deviation (RMSD) is a standard distance measure between coordinates. This diagram illustrates the charge in protein conformation during MD simulation. The root-mean-square fluctuation (RMSF) indicates the variation of protein residues over time relative to a reference position during simulation. The H-bond plot demonstrates the number of H-bond interactions between the protein and ligand during simulation.

2.10. Codon optimization and in silico cloning

We obtained the engineered vaccine's cDNA using the GenScript server (https://www.genscript.com/tools.html). Java Codon Adaptation Tool (JCat) was utilized to optimize codon usage by Escherichia coli (*E. coli*) [78], which computes the proportion of GC content and codon adaptation index (CAI) to estimate the expression ability of the cloned sequence. In addition, *E. coli* K12 was employed to evaluate vaccine expression efficiency. The optimized vaccine was cloned using restriction enzymes and the Snapgene (https://www.snapgene.com/) software. The *E. coli* pET 30A + plasmid was obtained using the Addgene server (https://www.addgene.org/).

2.11. Immune stimulation

The C-ImmSim server (https://150.146.2.1/C-IMMSIM/index.php) was used to illustrate the cellular and humoral responses of the mammalian immune system, as well as the immunogenic potential of the multi-epitope vaccine [79]. This server stimulates the immunological interactions of the predicted epitopes using a position-specific score matrix (PSSM), the Celada-Seide model, and several other machine-learning techniques. After vaccination injection, the C-ImmSim server estimates the levels of various factors, including T-cell 1 (Th1), helper T-cell 2 (Th2), interferon, cytokines, and antibodies. The stimulation of this server corresponds to three major anatomical locations in the mammalian immune system: 1) the bone marrow, 2) the thymus, and 3) tertiary lymphatic organs, including the tonsil, spleen, and lymph nodes [79]. The literature recommends a minimum interval of four weeks between vaccinations, but this interval can be extended to three to six months [19,80]. Consequently, we analyzed the vaccine's immune response by administering three injections at a 4-week interval.

3. Results

3.1. Protein target sequence retrieval

In this study, five protein sequences, A34L, A29L, B14R, E13L, and A27L, were obtained from the UniProt server (Table 3) and used to create a multi-epitope vaccine against MPXV. The specified parameters are shown in Table 2. Other parameters were set as the server's defaults. After examining the studied sequences, the selected epitopes were

Fig. 4. The final design of the monkey virus multi-epitope vaccine (from left to right). The basic structure of the designed vaccine in the form of single-letter amino acid, including adjuvants, linkers and epitopes, respectively.

Table 5
Predicted CTL epitopes with high safety and suitable conditions for designing multi-epitope vaccine constructs.

CTL Epitope	Alleles	Vaxigen	Antigenicity	Allergenicity	Immunogenicity	Toxicity	Combined score	Virulence potential	Solubility
FLFLNINHY (A27L)	A1, A3, A26, B62	1.1282	Antigen	Non-allergen	0.15926	Non-toxin	1.1307	Virulent	PWS*
KSGDLKYTY (A27L)	A1, B58, B62	1.6991	Antigen	Non-allergen	−0.16092	Non-toxin	1.3972	Virulent	GWS*
LTRKTRNVI (A27L)	B7, B8	1.2115	Antigen	Non-allergen	−0.09502	Non-toxin	0.7785	Virulent	GWS
RTVIGIADY (A27L)	A1, A3, A26, B58, B62	1.0792	Antigen	Non-allergen	0.35158	Non-toxin	1.2649	Virulent	GWS
SRLQSRISD (A27L)	B27	1.1119	Antigen	Non-allergen	−0.21688	Non-toxin	0.7531	Virulent	GWS
KWPLLNIGI (A29L)	A24	1.3057	Antigen	Non-allergen	0.10047	Non-toxin	1.2143	Virulent	PWS
TIIDPDFVF (A29L)	A26, B58, B62	1.5033	Antigen	Non-allergen	0.19852	Non-toxin	1.1342	Virulent	PWS
TREMGFLVY (A29L)	A1, B27, B39	1.0515	Antigen	Non-allergen	0.01376	Non-toxin	0.9198	Virulent	PWS
ARSNNRLAI (A34L)	B7, B27, B39	1.0338	Antigen	Non-allergen	−0.00429	Non-toxin	0.7516	Virulent	GWS
FTPVYNPDY (A34L)	A1, A26, B62	0.5907	Antigen	Non-allergen	0.03185	Non-toxin	2.6108	Virulent	PWS
LIYYQINLV (A34L)	A2	1.0381	Antigen	Non-allergen	−0.00438	Non-toxin	1.0204	Virulent	GWS
YIWPNHINF (A34L)	A26, B58, B62	0.9089	Antigen	Non-allergen	0.19343	Non-toxin	0.8542	Virulent	PWS
DMMSLNLTI (B14R)	A2, A24	1.3725	Antigen	Non-allergen	−0.22704	Non-toxin	0.7989	Virulent	GWS
ITCRVSLRL (B14R)	B58	1.6378	Antigen	Non-allergen	−0.06007	Non-toxin	1.0678	Virulent	GWS
LEVRDRIIP (B14R)	B44	2.1541	Antigen	Non-allergen	0.32588	Non-toxin	0.7818	Virulent	GWS
SLNLTIVSV (B14R)	A2	1.9014	Antigen	Non-allergen	0.088	Non-toxin	1.1232	Virulent	PWS
ELNDISIGL (E13L)	A2, A26	2.5692	Antigen	Non-allergen	0.12621	Non-toxin	0.9126	Virulent	GWS
FEIRDQYIT (E13L)	B44	2.2067	Antigen	Non-allergen	0.08248	Non-toxin	0.7921	Virulent	GWS
GTRKNSFIY (E13L)	A1, A3, A26, B62	0.6851	Antigen	Non-allergen	−0.18567	Non-toxin	1.4676	Virulent	GWS
KNVQIKPSF (E13L)	B58	1.5698	Antigen	Non-allergen	−0.28258	Non-toxin	0.8214	Virulent	GWS
LTFNFTPKI (E13L)	A2	2.1767	Antigen	Non-allergen	0.04667	Non-toxin	0.94	Virulent	PWS
TIALKHSGY (E13L)	A1, A3, A26, B62	1.1727	Antigen	Non-allergen	−0.29783	Non-toxin	1.3052	Virulent	PWS
VPYVGYKCI (E13L)	B7	1.2837	Antigen	Non-allergen	−0.14364	Non-toxin	0.8028	Virulent	PWS

*PWS: poor water solubility, *GWS: good water solubility.

examined. Antigenicity scores obtained from the VaxiJen v2.0 and ANTIGENpro servers indicated that the chosen proteins were antigenic. AllerTOP v. 2.0 and the Toxinpred server confirmed the non-allergenic and non-toxic nature of the proteins, respectively. The VirulentPred web server revealed that all sequences were involved in virulence (Table 4).

3.2. T-cell epitope prediction and selection

The NetCTL 1.2 server analysis predicted 9-mer CTL lymphocytes epitopes, identifying 148 epitopes for A27L, 88 epitopes for A29L, 71 epitopes for B14R, 126 epitopes for B13L, and 84 epitopes for A34L. Similarly, the NetMHCII 2.3 server was used to predict HTL lymphocytes epitopes (15-mer), yielding 41 epitopes for A29L, 57 for B14R, 119 for E13L, 121 for A34L, and 325 for A27L. Antigenicity, allergenicity, toxicity, IFN-γ, IL-4, and IL-10 induction were screened for in human MHC II alleles. The epitopes were subjected to the prediction of interferon-gamma (IFN), a cytokine that can stimulate the host's innate and acquired immune responses, including macrophages and natural killer cells. IFNepitope prediction server utilizes motif and support vector machine (SVM) hybrid and IFN versus other cytokines as prediction models. This server uses a dataset that activates T helper cells through inducing and non-inducing MHC class II binders. In addition, we forecasted the solubility and virulence of CTL and HTL epitopes (Fig. 4). The epitopes were selected per the characteristics listed in Tables 5 and 6.

3.3. Prediction of linear and discontinuous B-cell epitopes

Predicting linear B-cell epitopes yielded 12 -mer B-cell epitopes for the targeted proteins. We obtained 72B-cell epitopes for A27L, 14B-cell epitopes for A29L, 28B-cell epitopes for B14R, 47B-cell epitopes for E13L, and 20B-cell epitopes for A34L (Table 7). After three-dimensional structural refinement, the ElliPro server predicted five discontinuous B-cell epitopes with a range of 7 to 41 amino acids for the designed vaccine (Fig. 5). The scores ranged from 0.719 to 0.797. The minimum score was set at 0.5, and the maximum distance was set at 6 Å (Table 8).

3.4. Vaccine structure design

The vaccine construct was designed using 13 linear B-cell epitopes (Table 7), 23 MHC-I epitopes (Table 5), and 11 MHC-II epitopes (Table 6). GPGPG linkers for HTL epitopes, AAY linkers for CTL epitopes, and KK linkers for B lymphocytes were used to connect a subset of

Table 6
Predicted HTL epitopes with high safety and suitable conditions for designing multi-epitope vaccine constructs.

HTL epitope	Alleles	Vaxigen	Antigenicity	Allergenicity	Toxicity	Hydrophobicity	Hydropathicity	Hydrophilicity	Charge	IFN-gamma	IL-10	IL-4	Virulent potential	Solubility
SGGGNLTEISRLQSR (A27Lb: 662 a)	DRB1_0801, DRB1_0803, DRB1_1101, DRB1_1104, DRB1_1301, DRB1_1302, DRB1_1303, DRB1_1401, DRB1_1402, DRB1_1454	0.769	Antigen	Non-allergen	Non-toxin	−0.28	−0.78	0.3	1	Positive	IL10 Inducer	IL4 Inducer	Virulent	GWS
HRELEEERRHVRDLE (A27L: 612)	DRB1_0301, DRB1_1301, DRB1_1302	0.7635	Antigen	Non-allergen	Non-toxin	−0.67	−2.24	1.59	−1	Positive	IL10 Inducer	IL4 Inducer	Virulent	GWS
LKMPFRMVLTGGSGS (A34L: 45)	DRB1_0401, DRB1_0402, DRB1_0403, DRB1_0404, DRB1_0405, DRB1_0408, DRB1_0801, DRB1_1001, DRB1_1101, DRB1_1601, DRB5_0101	0.7976	Antigen	Non-allergen	Non-toxin	−0.03	0.33	−0.27	2	Positive	IL10 Inducer	IL4 Inducer	Virulent	PWS
SFNISISDAENMLRS (A34L: 189)	DRB1_0701, DRB1_0901	0.7266	Antigen	Non-allergen	Non-toxin	−0.15	−0.16	0.06	−1	Positive	IL10 Inducer	IL4 Inducer	Virulent	GWS
SKCNTLIEFLNFGRH (A34L: 147)	DRB5_0202	0.7238	Antigen	Non-allergen	Non-toxin	−0.16	−0.25	−0.17	1.5	Positive	IL10 Inducer	IL4 Inducer	Virulent	PWS
CSFNISISDAENMLR (A34L: 188)	DRB1_0701	0.5080	Antigen	Non-allergen	Non-toxin	−0.13	0.06	−0.03	−1	Positive	IL10 Inducer	IL4 Inducer	Virulent	GWS
NEETLKQRLTNLEKK (A29L: 43)	DRB1_0402, DRB1_0801, DRB1_0803	0.5607	Antigen	Non-allergen	Non-toxin	−0.51	−1.81	1.03	1	Positive	IL10 Inducer	IL4 Inducer	Virulent	GWS
RLEVRFGNDVLYSEN (E13L: 442)	DRB1_1201	1.0386	Antigen	Non-allergen	Non-toxin	−0.27	−0.68	0.29	−1	Positive	IL10 Inducer	IL4 Inducer	Virulent	GWS
TDIISRLEVRFGNDV (E13L: 437)	DRB1_0404,DRB1_0402	0.7819	Antigen	Non-allergen	Non-toxin	−0.19	−0.06	0.28	−1	Positive	IL10 Inducer	IL4 Inducer	Virulent	GWS
VFAHISHTINIIDTS (E13L: 380)	DRB1_0405	0.8974	Antigen	Non-allergen	Non-toxin	0.09	0.69	−0.65	0	Positive	IL10 Inducer	IL4 Inducer	Virulent	PWS
KTDIISRLEVRFGND (E13L: 436)	DRB1_1201, DRB1_1301, DRB4_0101, DRB4_0103	0.8985	Antigen	Non-allergen	Non-toxin	−0.3	−0.6	0.58	0	Positive	IL10 Inducer	IL4 Inducer	Virulent	GWS

a: Position, b: Gene name.

Table 7
Linear B-cell epitopes selected for multi-epitope vaccine design.

Protein	Position	Name	Linear B cell epitope	Predictive server	Vaxigen	Antigenicity	Allergenicity	Toxicity	Molecular weight	Virulent potential	Solubility
A27L	223–234	B Cell 1 A27L	LAPTDLGLALSK	ABCpred Prediction server	1.8896	Antigen	Non-allergen	Non-toxin	1198.6	Virulent	Soluble
A27L	30–41	B Cell 2 A27L	SSESGLTRKTRN	IEDB Analysis Resource Chou & Fasman Beta-Turn Prediction	1.0134	Antigen	Non-allergen	Non-toxin	1335.6	Virulent	Soluble
A27L	658–669	B Cell 3 A27L	DCIESGGGNLTE	IEDB Analysis Resource Chou & Fasman Beta-Turn Prediction	0.5232	Antigen	Non-allergen	Non-toxin	1194.41	Virulent	Soluble
A34L	221–233	B Cell 1 A34L	QRQVPVVGINGK	ABCpred Prediction server	1.2055	Antigen	Non-allergen	Non-toxin	1294.71	Virulent	Soluble
A34L	234–246	B Cell 2 A34L	SEYHAAVGHALL	ABCpred Prediction server	0.4587	Antigen	Non-allergen	Non-toxin	1267.58	Virulent	Soluble
A29L	56–67	B Cell 1 A29L	NNSNSTTPTTKS	ABCpred Prediction server	0.6341	Antigen	Non-allergen	Non-toxin	1251.43	Virulent	Soluble
B14R	47–58	B Cell 1 B14R	AMQVADRCHVIA	ABCpred Prediction server	1.0779	Antigen	Non-allergen	Non-toxin	1313.72	Virulent	Soluble
B14R	87–98	B Cell 2 B14R	LNPTQSDSGIYI	IEDB Analysis Resource Chou & Fasman Beta-Turn Prediction	0.7545	Antigen	Non-allergen	Non-toxin	1307.6	Virulent	Soluble
B14R	151–162	B Cell 3 B14R	SSNVNADIIWSG	IEDB Analysis Resource Chou & Fasman Beta-Turn Prediction	0.4229	Antigen	Non-allergen	Non-toxin	1262.51	Virulent	Soluble
E13L	137–148	B Cell 1 E13L	DISIGLTPNDTI	ABCpred Prediction server	1.8776	Antigen	Non-allergen	Non-toxin	1258.57	Virulent	Soluble
E13L	377–388	B Cell 2 E13L	KRTVFAHISHTI	ABCpred Prediction server	0.7198	Antigen	Non-allergen	Non-toxin	1409.83	Virulent	Soluble
E13L	498–507	B Cell 3 E13L	RGKDKLSVRVVY	BCPREDS Server, AAP (Chen et al., 2007)	1.1793	Antigen	Non-allergen	Non-toxin	1419.86	Virulent	Soluble
E13L	57–68	B Cell 4 E13L	EIRDQYITALNH	BCPREDS Server, AAP (Chen et al., 2007)	1.1303	Antigen	Non-allergen	Non-toxin	1472.8	Virulent	Soluble

epitopes from the previous step. The adjuvants used were β-defensin-3: hBD-2 (PDB ID: 1FD3), sequence: (GIGDPVTCLKSGAICHPVFCPRRYK-QIGTCGLPGTKCCKKP), and C205H340N60O53: LL-37, antimicrobial peptides (AMPs) with human sequence: (LLGDFFRKSKE-KIGKEFKRIVQRIKDFLRNLVPRTES) were attached to the N-terminal of the vaccine sequence through EAAAK linker (Fig. 3 and Fig. 4). A sequence of 749 amino acids was obtained after epitope and adjuvant fusion.

3.5. Physiochemical properties, antigenicity, allergenicity, toxic, and interferon-g activation potential of the designed vaccine

The results from the Protparam server indicated that the molecular weight of the vaccine structure was 82.15 kDa and that its theoretical pI was 9.66, rendering it an alkaline and stable structure with an instability index of 31.40 (an index below 40 is considered stable) [81]. The aliphatic index of the vaccine sequence was 83.55, and the GRAVY rate was −0.307, indicating that the vaccine construct exhibited excellent thermostability and hydrophilicity. The structure had a half-life of 30 h in mammals, estimated to be over 20 h in yeast and over 10 h in *E. coli*. The highly soluble nature of the vaccine construct was determined by the solubility scores of 0.791263 and 0.7729 for SOLpro and SoluProt v1 servers, respectively. The antigenicity and allergenicity of the final sequence of the candidate vaccine structure determined the vaccine's antigenic (0.7974; Vaxijen score and 0.7636; ANTIGENpro score) and non-allergenic behavior (Table 9).

3.6. Population coverage

The population coverage rate of the anticipated epitopes of A27L, A29L, B14R, E13L, and A34L proteins was analyzed by providing the MHC I and MHC II class of selected epitopes with their respective HLA alleles (listed in Table 10 and Table 11).

3.7. Vaccine construct secondary and tertiary structure prediction

The Prabi servers facilitated the prediction of the second structure of the vaccine construct by PSIPRED and SOPMA tools. In contrast, the PSIPRED server predicted 41.25% alpha helices, 16.95% extended strands, and 41.25% random coils (Fig. 6A). SOPMA predicted that the second structure of the vaccine would be composed of 34.58% alpha helix, 22.56% extended strands, and 35.38% random coils (Fig. 6B). The Prabi server additionally predicted 39.12% alpha helices, 17.49% extended strands, and 43.39% random coils (Fig. 6C). A high percentage of random coils indicated the greater flexibility of the vaccine structure.

Based on I-TASSER, PS2 servers, and the C score, the predicted tertiary structure is between −2 and −5. The results revealed ten threading templates with five top models (c-scores: −2.06, −1.33, −2.66, −4.81, and −4.78), whereas a C-score with a high value indicated a model with high confidence [82]. The top model (model 1) with the highest score (-2.06) was selected and optimized by GalaxyRefine (Fig. 7). The estimated TM-score and RMSD for the selected model were 0.47 ± 0.15 and 13.3 ± 4.1 Å, respectively. Galaxy web server was used to refine model 1 obtained from I-TASSER and PS2 protein predictor servers.

Ramachandran plot analysis, ProSA-web (Fig. 9A, 9B, 10B), ERRAT

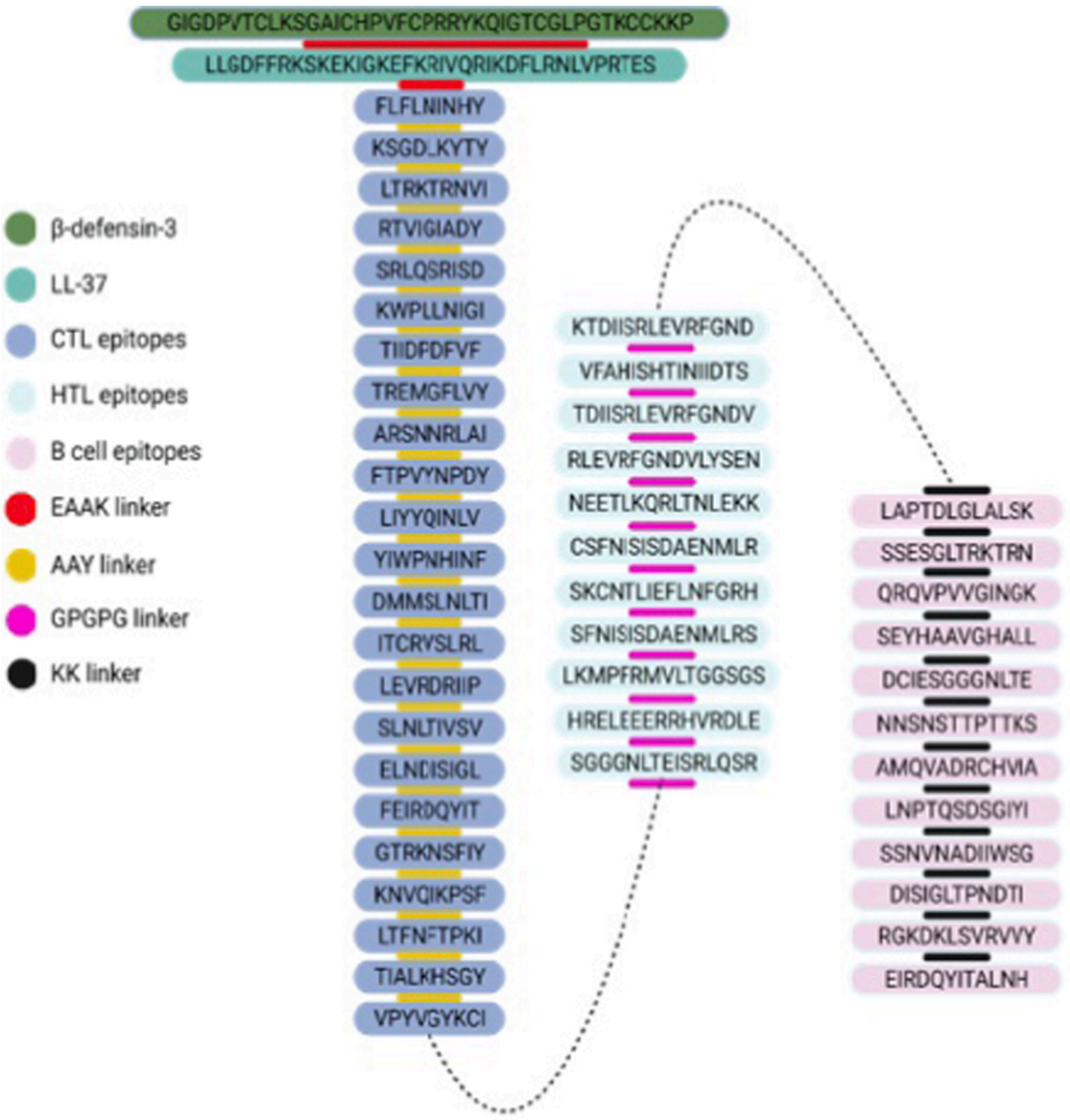

Fig. 5. Schematic representation of the subunit vaccine construct design.

(Fig. 10A), and Verify 3D were utilized in the structural validation process by comparing the potential errors and quality of the initial tertiary structure model before (Fig. 8A) and after (Fig. 8B) structural validation (Fig. 10C). In the initial model, the PROCHECKER server's Ramachandran plot analysis revealed that 1,497 (78.391%) of the residues were in the most favored region, 88 (13.880%) were in additional allowed regions, and 49 (7.729%) were in generously allowed regions. Following refinement, the recombinant vaccine contained 597 (94.164%) residues in the most favored region, 28 (4.416%) residues in additional allowed regions, and 9 (1.420%) residues in generously allowed regions.

According to the ERRRAT server, the initial model had an overall quality factor of 79.063, whereas the final model had an overall quality factor of 81.983. The ProSA-web server was utilized to assess the potential and quality errors in the 3D crude model. This server performed Z-score prediction, which was determined to be −5 in the initial model (Fig. 9A) and −5.6 after refinement (Fig. 9B). The low Z-score ensures the model's superior quality.

3.8. Molecular docking with TLRs

Considering the significance of the molecular association between each vaccine candidate and the host immune receptor in inducing a protective immune response, the ClusPro v2 server was used to investigate the binding affinity of this multi-epitope vaccine with TLR-3 and TLR-4 receptors. Cluster 0 of TLR3 was selected for molecular dynamics simulation analysis due to its lowest energy structure (-1098.9 kcal/mol) and highest member count (88). Cluster 0 of TLR4 was selected for molecular dynamics simulation analysis due to its lowest energy structure (-1100.07 kcal/mol) and the highest number of members, 45, indicating the highest binding affinity (Fig. 11).

3.9. MD simulation

The TLR-vaccine structures resulting from molecular docking were evaluated through MD simulation. GROMACS 4.6.5 was used to perform structural refinement. Complexes were centered in a box and filled with water using the tip3 water model. For neutralization, some water molecules were randomly replaced with ions. The systems were simulated using an ensemble of NPT and NVT with periodic boundary

Table 8
Discontinuous B-cell epitopes selected for multi-epitope vaccine design.

Residues	Number of residues	Score
A:G1, A:I2, A:G3, A:D4, A:P5, A:V6, A:T7, A:I143, A:S144, A:A147, A:Y148, A:P151, A:L152, A:L153, A:N154, A:I155, A:I157, A:A158, A:A159, A:Y160, A:T161, A:I162, A:I163, A:D164, A:P165, A:D166, A:Y211, A:Y212, A:Q213, A:I214, A:N215, A:L216, A:V217, A:A218, A:A219, A:Y220, A:Y221, A:I222, A:I227, A:N228, A:I264	41	0.755
A:A679, A:K680, A:V733, A:V734, A:Y735, A:K736, A:K737, A:E738, A:I739, A:R740, A:D741, A:Q742, A:I744, A:T745, A:A746, A:L747, A:N748, A:H749	18	0.797
A:G590, A:L591, A:A592, A:L593, A:S594, A:K595, A:K596, A:K597, A:S598, A:S599, A:E600, A:S601, A:G602, A:L603, A:T604, A:R613, A:Q614, A:V615, A:P616, A:V617, A:V618, A:G619, A:I620, A:N621, A:S656, A:S658, A:T660, A:P661, A:T662, A:T663	30	0.773
A:A185, A:R186, A:S187, A:N188, A:N189, A:R190, A:L191, A:A192, A:I193, A:A194, A:L237, A:N238, A:L239, A:V259, A:R260	15	0.719
A:P586, A:K606, A:T607, A:R608, A:N609, A:K610, A:K611	7	0.797

Table 9
Basic characteristics of the vaccine structure designed against monkey pox.

Population/Area	MHC I epitope	Coverage[a]	Average_hit[b]	Pc90[c]
World	FLFLNINHY	39.95%	0.43	0.17
World	KSGDLKYTY	22.98%	0.24	0.13
World	LTRKTRNVI	24.48%	0.25	0.13
World	RTVIGIADY	43.49%	0.49	0.18
World	SRLQSRISD	8.05%	0.08	0.11
World	KWPLLNIGI	26.14%	0.27	0.14
World	TIIDPDFVF	12.71%	0.13	0.11
World	TREMGFLVY	39.73%	0.46	0.17
World	ARSNNRLAI	38.5%	0.42	0.16
World	FTPVYNPDY	28.77%	0.3	0.14
World	LIYYQINLV	45.08%	0.47	0.18
World	YIWPNHINF	12.71%	0.13	0.11
World	DMMSLNLTI	63.94%	0.74	0.28
World	ITCRVSLRL	5.9%	0.06	0.11
World	LEVRDRIIP	15.38%	0.16	0.12
World	SLNLTIVSV	45.08%	0.47	0.18
World	ELNDISIGL	53.71%	0.59	0.22
World	FEIRDQYIT	15.38%	0.16	0.12
World	GTRKNSFIY	53.58%	0.61	0.22
World	KNVQIKPSF	5.9%	0.06	0.11
World	LTFNFTPKI	45.08%	0.47	0.18
World	TIALKHSGY	39.95%	0.43	0.17
World	VPYVGYKCI	14.23%	0.14	0.12

[a] Projected population coverage.
[b] Average number of epitope hits / HLA combinations recognized by the population.
[c] Minimum number of epitope hits / HLA combinations recognized by 90% of the population.

conditions. Using the Parrinello-Rahman algorithm, 1 pressure bar was set under isotropic conditions. PME [74] computed electrostatic interactions, and the LINCS procedure [75] was used to constrain all hydrogen-atom-bonding bonds.

After neutralization, the steepest descent algorithm was employed for energy minimization. 100 ps of MD equilibration was performed with positional restraints on protein-heavy atoms with a spring constant of 1000 kcal.mol^{-1}nm^{-2} to prevent non-physical conformational changes in the solvated protein. The final MD simulation ran for 100 ns without restriction. RMSD is a standard measure of the distance between coordinates. During the MD simulation, the conformational change of the protein is depicted in this plot.

In the RMSD plot of TLR4, an upward trend was established at approximately 0.4 nm from 65 ns at the start of the simulation and

Table 10
Population coverage of selected MHC I epitopes for overall world population.

Proprety	Result
Allergenicity (AllerTOP v. 2.0)	Non-allergic
Allergenicity (AllergenFP v.1.0)	Non-allergic
Antigenecity (VaxiJen v2.0), score	Antigen, 0.7974
Antigenecity (ANTIGENpro), score	Antigen, 0.7636
Predicted solubility upon overexpression (scratch), score	Soluble, 0.791263
Solubility (Soluprot), score	Soluble, 0.773
Codon optimization index GenScrip/ JCat	0.84/1
Aliphatic index	83.55
Stability index (II)	Stable, 31.40
Expression vector	E. coli pET 30A+
Theoretical pI	9.66 (alkaline)
Number of Amino acids	749
Half-Life	30 h (mammalian reticulocytes, in vitro) >20 h (yeast, in vivo) >10 h (Escherichia coli, in vivo)
Formula	$C_{3687}H_{5831}N_{1027}O_{1060}S_{20}$
GRAVY	−0.307

Table 11
Population coverage of selected MHC II epitopes for overall world population.

Population/Area	MHC II epitope	Coverage[a]	Average_hit[b]	Pc90[c]
World	SGGGNLTEISRLQSR	45.4%	0.51	0.18
[97]	HRELEEERRHVRDLE	31.53%	0.33	0.15
World	LKMPFRMVLTGGSGS	41.06%	0.46	0.17
World	SFNISISDAENMLRS	24.01%	0.25	0.13
World	SKCNTLIEFLNFGRH	43.56%	0.48	0.18
World	CSFNISISDAENMLR	18.23%	0.18	0.12
World	NEETLKQRLTNLEKK	7.97%	0.08	0.11
World	RLEVRFGNDVLYSEN	4.47%	0.04	0.1
World	TDIISRLEVRFGNDV	6.54%	0.07	0.11
World	VFAHISHTINIIDTS	7.71%	0.08	0.11
World	KTDIISRLEVRFGND	27.59%	0.29	0.14

[a] Projected population coverage.
[b] Average number of epitope hits / HLA combinations recognized by the population.
[c] Minimum number of epitope hits / HLA combinations recognized by 90% of the population.

persisted until the end. The RMSD plot of the vaccine increased at the start of the simulation period, reaching 1.2 nm after 10 ns and 1.43 nm after 34 ns. Following this, the distance decreased to 1.1 nm in 71 ns. After this point, the RMSD value increased continuously at a rate of 1.8 nm per 92 ns and remained constant until the conclusion of the simulation (Fig. 12A). From 67 ns until the end of the simulation, the RMSD plot of TLR3 displayed an upward trend of approximately 0.4 nm beginning at the beginning of the simulation. The vaccine's RMSD plot established an increasing trend at approximately 1.1 nm from 25 ns and then decreased to 0.8 nm at 30 ns. The RMSD value increased continuously at 1.3 nm in 37 ns and remained constant until the end of the simulation (Fig. 12B).

The RMSF represents the fluctuation of protein residues over time, relative to a position of reference, during simulation. Fluctuations in the RMSF diagram of TLR4 were very mild (Fig. 12C). In contrast, the RMSF diagram of the vaccine exhibited severe fluctuations, with the highest peaks having a value of 0.6 nm, indicating a highly flexible region (amino acids 707–713) in the structure of the vaccine (Fig. 11D). Fluctuations in the RMSF diagram of TLR3 were very mild (Fig. 12E); however, fluctuations in the RMSF diagram of the vaccine were relatively strong, with the highest peaks with a value of 0.64 nm indicating the highly flexible region (amino acids 704–710, and 711–715) in the vaccine structure (Fig. 12F). During MD simulations, hydrogen bonds were analyzed between TLR4 and the vaccine complex (Fig. 12G) and between TLR3 and the vaccine complex (Fig. 12H).

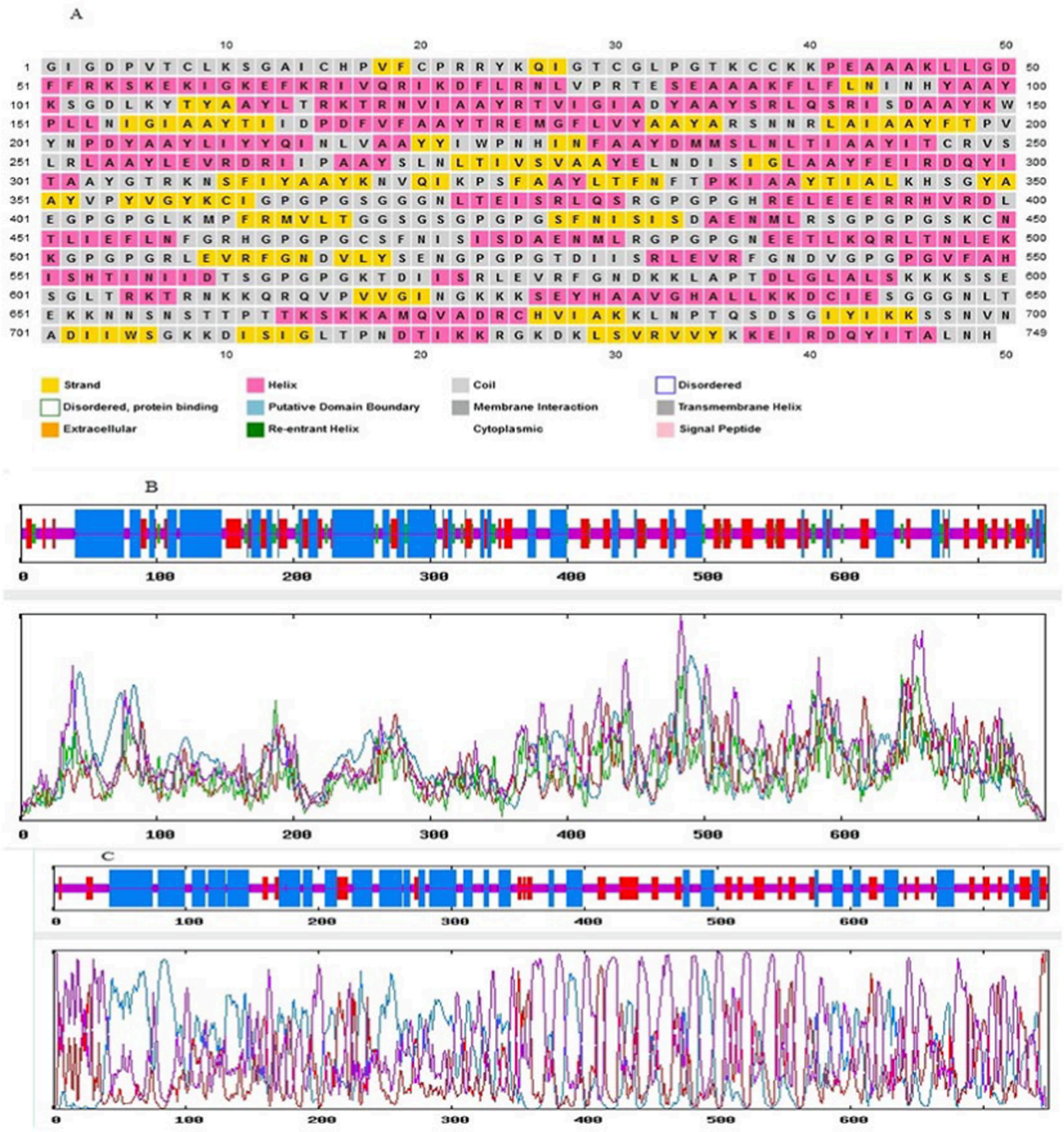

Fig. 6. Predicted schematic image of the secondary structure of the multi-epitope vaccine by: (A) PSIPRED server, (B) SOPMA server, (C) Prabi server.

3.10. Immune stimulation

The C-ImmSim server performed in silico immune stimulation of the potential vaccine candidate via primary and secondary immune responses by activating immune system components, including HTL, CTL, viable memory cells, and other associated immune cells (Natural killer [NK] cells and dendritic cells [DCs], among others). Immunoglobulin levels (IgM + IgG) increased significantly following administration of the subunit vaccine. Through the high titers of IgM and IgG, significant immune responses were observed against the monkeypox virus (Fig. 12A).

During the acting and resting phases, the innate immunity of the host and B-cell population was enhanced by 650–700 IgM, B isotype, and B-memory cells (Fig. 13A–C). Similarly, CTL cells were increased and reached a maximum of 1103 cells/next ~ 8 days of immunization with vaccine before decreasing gradually over the following 20 days (Fig. 13D). In addition, during the resting and active phases, the T-cell population displayed a high degree of diversity (Fig. 13E).

In addition, it was observed that the raised HTL cells (during the resting and active phases) played a crucial role in developing adaptive immunity against the MPXV infection. The raised cells generated the most memory cells (Fig. 13F–G). Memory cells significantly prevent and regulate viral infection and reinfection during self-memorization following pathogen exposure. The vaccine candidate's successful

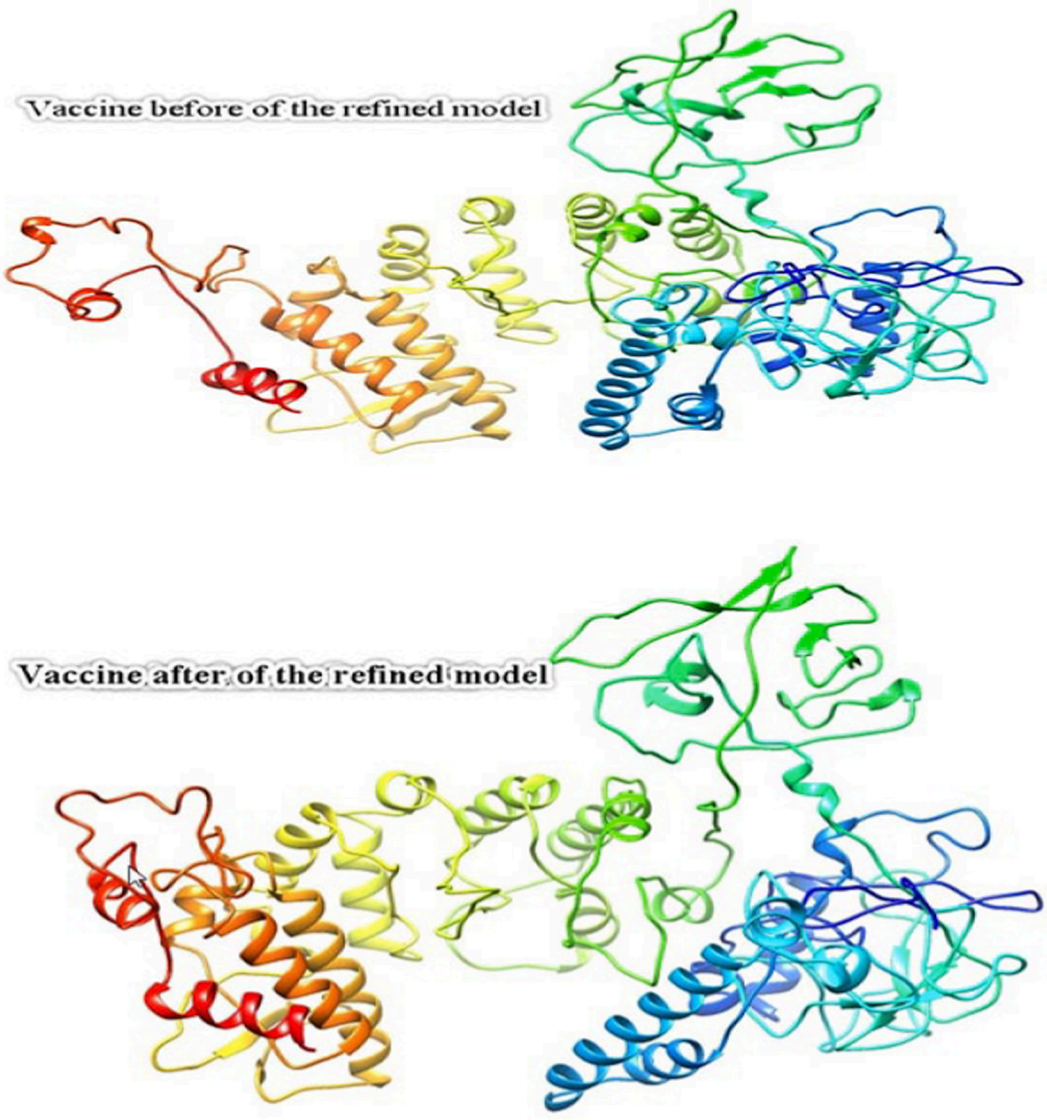

Fig. 7. The 3D figure of the multi-epitope of the newly designed vaccine before and after refinement.

administration increased the immune system's added regulatory components (e.g., interleukins, cytokines, and NK cells) (Fig. 13F-L). These findings suggest that the designed MPXV subunit vaccine is a potent multi-epitope peptide-based next-generation vaccine for inducing a robust immune response against MPXV infection.

3.11. Codon optimization and in silico cloning

The length of the cDNA sequence with an optimized codon of 2247 nucleotides was estimated using GenScript and JCat. The codon optimization of the vaccine structure utilizing the JCat server revealed the percentage of GC (the standard range is 30 to 70%) and the percentage of the codon compatibility index (the standard value of the compatibility index is 1). The results of codon optimization with the GenScript server revealed that the CAI values of the optimized sequences had a score of 0.84, and the GC content was 50.17 percent, indicating the high expression of vaccine antigens. *E. coli* K12 was utilized to enhance the efficiency of vaccine production. Finally, The optimized sequence was inserted using the SnapGene software into the expression vector pET 30A+ (Fig. 14).

4. Discussion

In several regions worldwide, the dsDNA orthopoxvirus MPXV has caused outbreaks and increased mortality rates in children and those with compromised immune systems. Since existing vaccines only offer partial protection against MPXV, developing more effective vaccines against the virus will necessitate using immunoinformatics approaches to design epitope-based subunits, which are becoming standard practice in first-line vaccine development [83]. Therefore, cutting-edge bioinformatics and therapeutic methods must be applied to the recently discovered MPXV infection. The availability of genetic and proteomic data and recent advances in reverse vaccinology can be used to develop multi-epitope vaccines for this purpose [84]. Therefore, a multi-epitope subunit vaccine was developed in this study to stimulate an immune response against MPXV by targeting the cell surface-binding protein.

Although smallpox and monkeypox are physiologically distinct diseases, they share many of the same characteristics as viral zoonotic diseases. The monkeypox virus, which causes the disease, is a major cause of public health concern in Africa [85]. Epitope-based vaccines represent a novel strategy for vaccine development due to their increased safety, effectiveness, and practicality. Vaccines using live or attenuated viruses have historically been effective but have also been

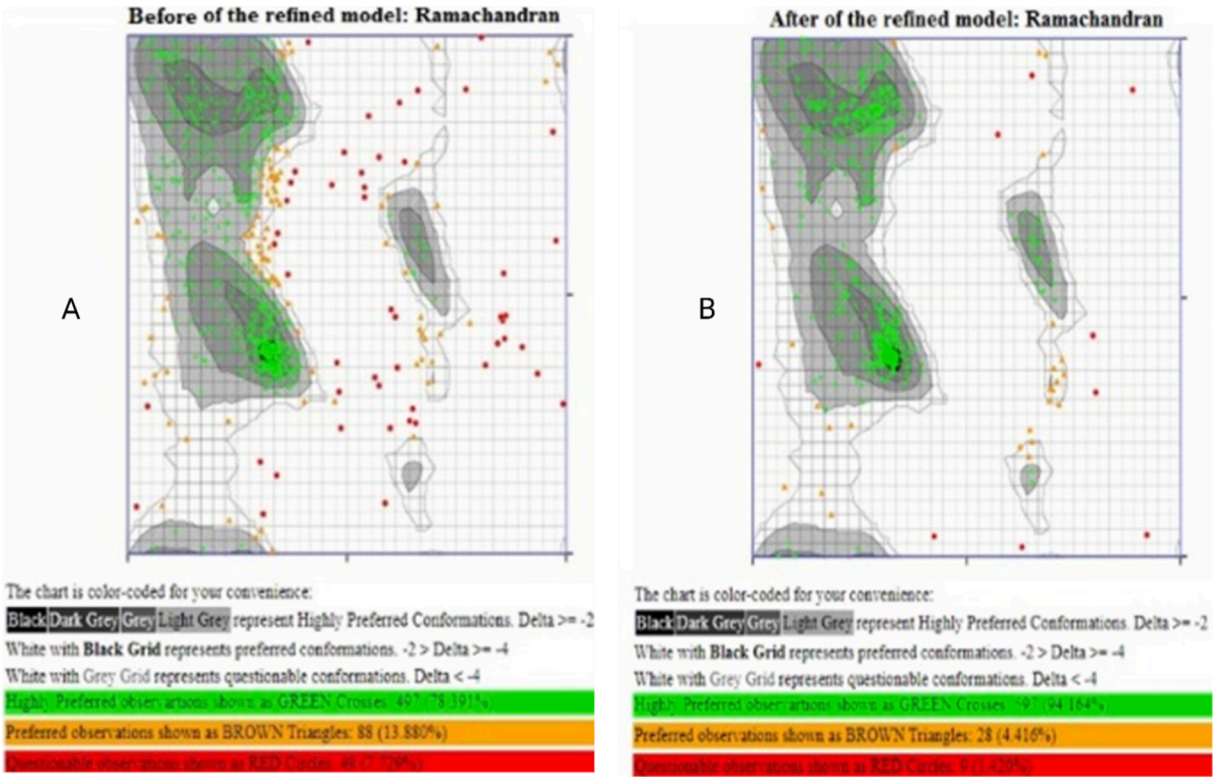

Fig. 8. (A) Ramachandran plot of vaccine before the refinement. The green crosses (78.391%) are the amino acid residues in most favored/allowed region, the brown triangles (13.88%) are the amino acid residues in favored region and the red dots (7.72%) are the residues in disallowed region. (B) Ramachandran plot of refined model of vaccine shows 94.164% of the amino acid residues in highly preferred region with green crosses. The brown triangles and red dots were 4.416% and 1.42%, respectively.

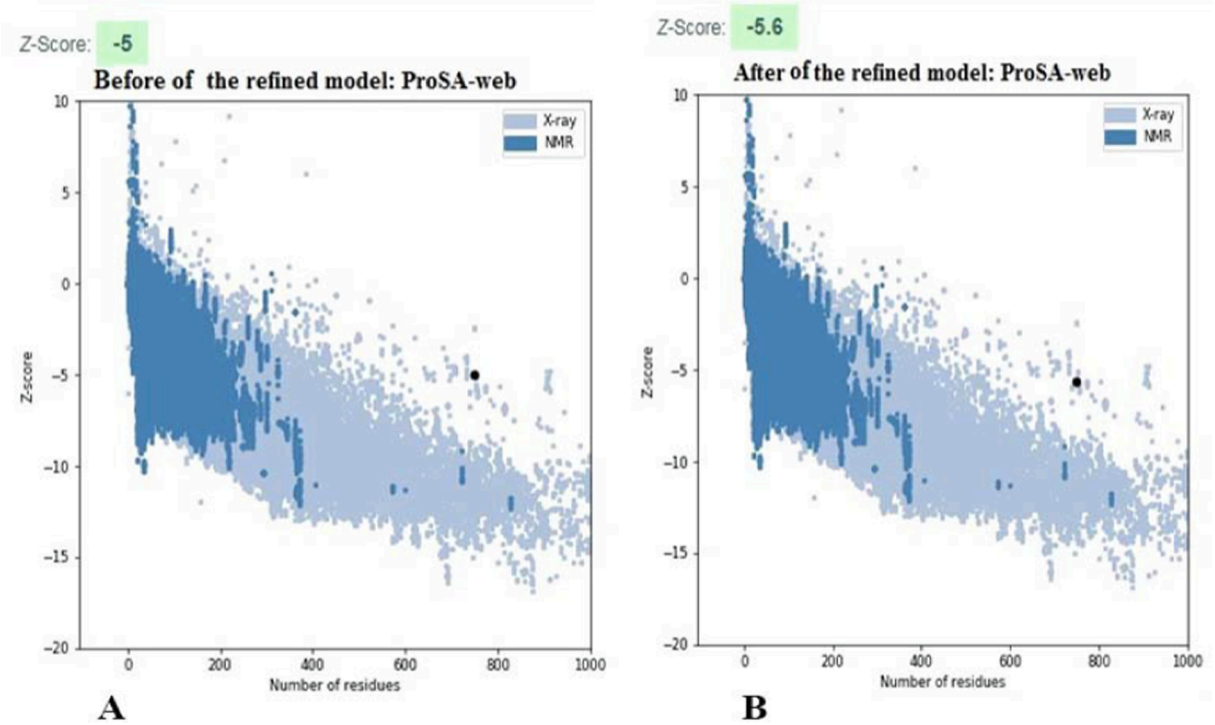

Fig. 9. This graph is generated by ProSAweb for vacccine showing the quality of 3D model on the basis of z-score for vaccine construct (A) before and (B) after refinement.

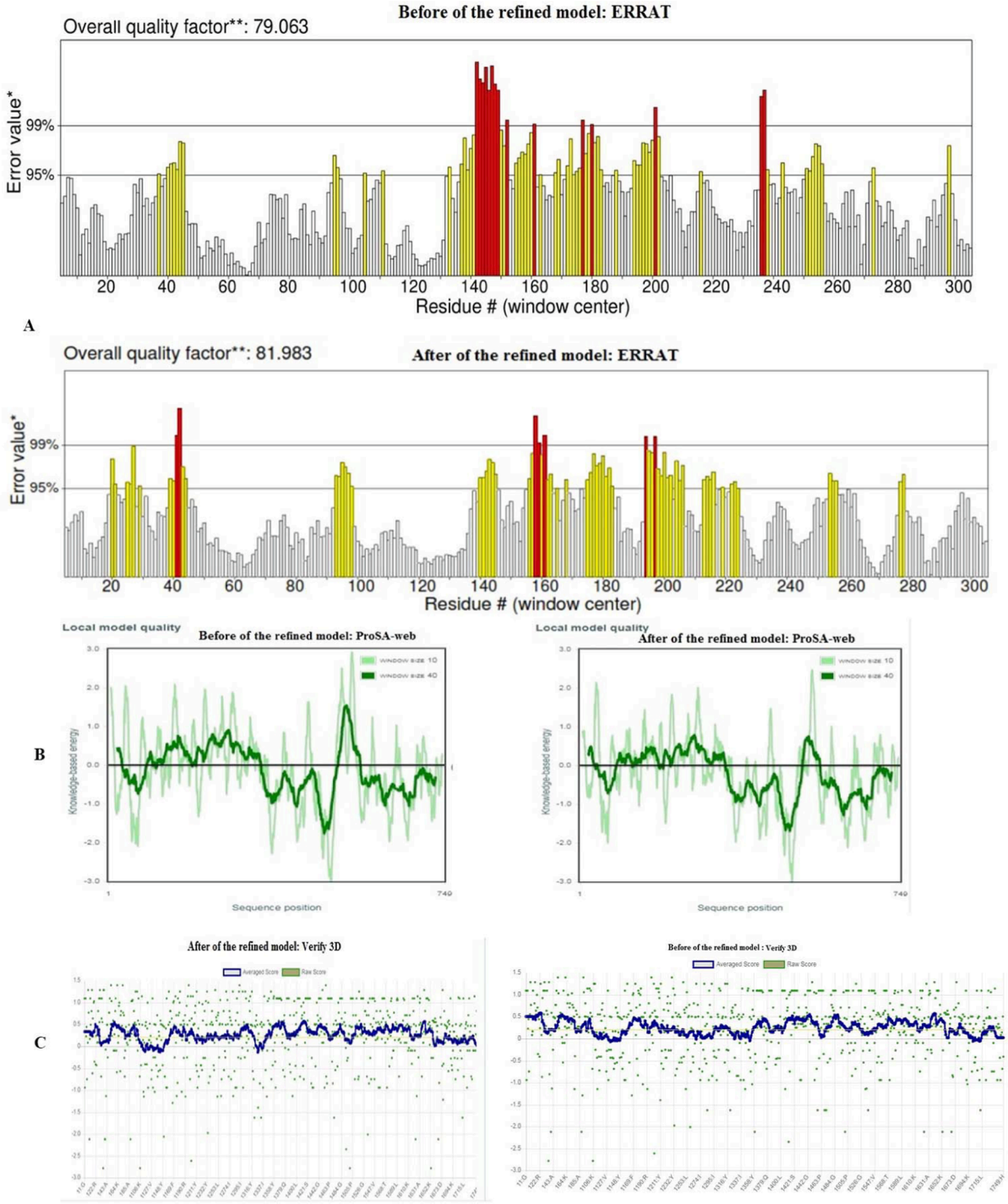

Fig. 10. The results of other several tertiary structure validation tools before and after refinement confirmed the modeled multi-epitope vaccine structure to be quite reliable and accurate. (A) ERRAT, (B) ProSA-web, and (C) verify3D.

associated with adverse immune responses. These biosafety concerns can be resolved with immunoinformatics methods without additional expense or delay. Vaccines that target multiple conserved epitopes within an antigenic sequence can elicit a protective immune response. The immune system can ignore potentially harmful antigens known as "unfavorable epitopes" that would otherwise trigger an immune response that could harm the host [86,87].

Detection of helper T-cell (HTL), CTL, and B-cell epitopes is essential for developing multi-epitope vaccines [88]. GPGPG, KK, and AAY Linkers were used to join HTL, CTL, and BCEs. Linkers were required to enhance the final vaccine's stability, folding, and expression [89]. In addition, an adjuvant can augment the immune response elicited by a subunit vaccine by activating TLRs on antigen-presenting cells, which may improve antibody recognition [90]. The "combination adjuvant" [91] is created by combining β-defensin-3 and LL37 to produce an adjuvant that is more antigenic without causing allergy symptoms and also induces a T helper-1-based adaptive immune response. T helper-1 lymphocytes are responsible for phagocyte activation and antibody-dependent cellular cytotoxicity, eliminating intracellular pathogens such as viruses [92]. Furthermore, the EAAAK linker was used between human β-defensin-3 and LL-37 and between LL-37 and the rest of the multi-epitope vaccine construct [93]. Moreover, β-defensin was

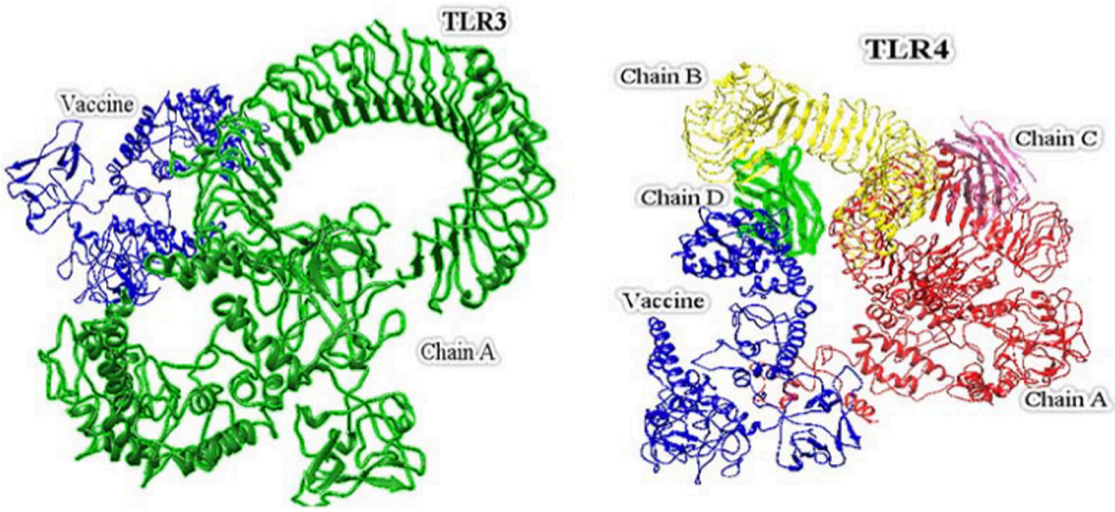

Fig. 11. Molecular docking of the vaccine with TLR3 and TLR4.

employed as an adjuvant due to its ability to function as both an antimicrobial and immunomodulatory agent.

β-defensin has been utilized in numerous studies on developing multi-epitope vaccines [94–96]. Recent research has demonstrated that the human antimicrobial peptide LL-37 is an effective adjuvant for an intranasal vaccine candidate against MERS-CoV infection [52,97]. In our research, two adjuvants significantly increased predicted antigenicity without causing allergic reactions. However, few viral vaccines employ peptide adjuvants or peptide combinations. In addition, predictions of cytokine response profiles induced by the combination of LL-37 and human β-defensin-3 and subsequent TLR3/TLR4 synergy have not been investigated. Therefore, additional research is required to determine the effect of the combination of these two adjuvants on immunogenicity.

This study also included five structural proteins of the monkeypox virus to develop a multi-epitope vaccine. Conserved T-cell epitopes were predicted using multiple sequence analysis, followed by IFN-γ, IL-10, IL-4, and B-cell epitopes. The antigenicity, allergenicity, and toxicity of these epitopes were evaluated subsequently. The vaccine could also increase the IFN-γ response, stimulating T helper cells to produce more robust immune responses [98]. Combining adjuvants enhanced the immunogenicity of multiple adaptive and innate immune mechanisms [99]. Regarding population coverage, the predicted T-lymphocyte-reactive epitopes were evaluated. Globally, epitopes may effectively interact with human alleles and cover a substantial population. A peptide must possess various physicochemical properties to operate effectively as a vaccine.

Based on the findings of this study, it was determined that the multi-epitope vaccine construct was hydrophobic and stable. It was determined that the multi-epitope vaccine has a basic pI, ensuring a stable interaction with the physiological pH. According to the aliphatic and instability indices, the protein of the vaccine may be thermostable and stable. The positive score for GRAVY indicates hydrophobicity. Therefore, the multi-epitope vaccine was immunogenic, non-allergenic, and antigenic to a high degree.

This concludes that the epitopic vaccine can elicit a robust immune response without triggering allergy symptoms. Analysis of vaccine constructs' secondary structure revealed alpha helices, extended strands, beta turns, and random coils. Using 3D structural predictions, the spatial arrangement of essential protein components can be better comprehended; this is an excellent tool for examining protein functions, other protein components, ligand–protein interactions, and protein dynamics. After refinement, the structure of the multi-epitope vaccine - significantly enhanced its desirable characteristics.

Ramachandran's plot analysis demonstrated that most residues were present in favored and allowed areas. Simultaneously, a negligible number was found in the disregarded sector, demonstrating the model's general accuracy. In addition to having poor rotamers, a low RMSD value, a high MolProbity, and a low clash score, the constructed multi-epitope vaccine was of high quality. Consequently, the ProSA program predicted model and structural errors. ProSA is utilized to evaluate the quality of input structures. Furthermore, amino acid scores were plotted, and negative values indicate the absence of structural model errors to evaluate the local model quality [100]. Based on the Z-score of the study, the proposed vaccine design against MPXV is satisfactory.

The interaction between antigens and immune receptors is required for immune activation [101]. Docking analysis was conducted between immune receptor molecules and epitopes to determine probable interactions, binding energy, and poses. The docking analysis was carried out using the ClusPro v2 server, which evaluates molecular surfaces, including solid molecular surfaces. TLR receptors play a crucial role in innate immunity by stimulating immune cells to induce adaptive immune responses. The final structure was docked against TLR3 to determine if appropriate binding to the immediate immune response was achieved. TLR3 enhances the infection's antiviral mechanism and locates infected cells that have died [102]. TLR4 is known to be involved in generating immune responses following viral infection, as its expression increases within a day of infection [103]. A TLR4 stimulation can also induce an immune response protective against Coronaviruses [104,105]. The TLR4 receptor was chosen based on studies with similar findings [106,107].

Because MEMPV combines multiple B- and T-cell epitopes, it should elicit substantial cellular and humoral immune responses. In addition, the immune system's response may vary depending on several variables, such as the pathogen's mechanism [41]. Therefore, the vaccine formulation was subjected to an analysis simulating the host's immune response [108]. The intended vaccine triggered all primary and secondary immune responses. The highest concentrations of antibodies were IgM + IgG, followed by IgM, IgG1 + IgG2, IgG1, and IgG2. Interleukin and cytokine induction was also analyzed and predicted.

We found that the proposed MEMPV construct was highly immunogenic. Still, monkeypox experiments must be conducted to determine

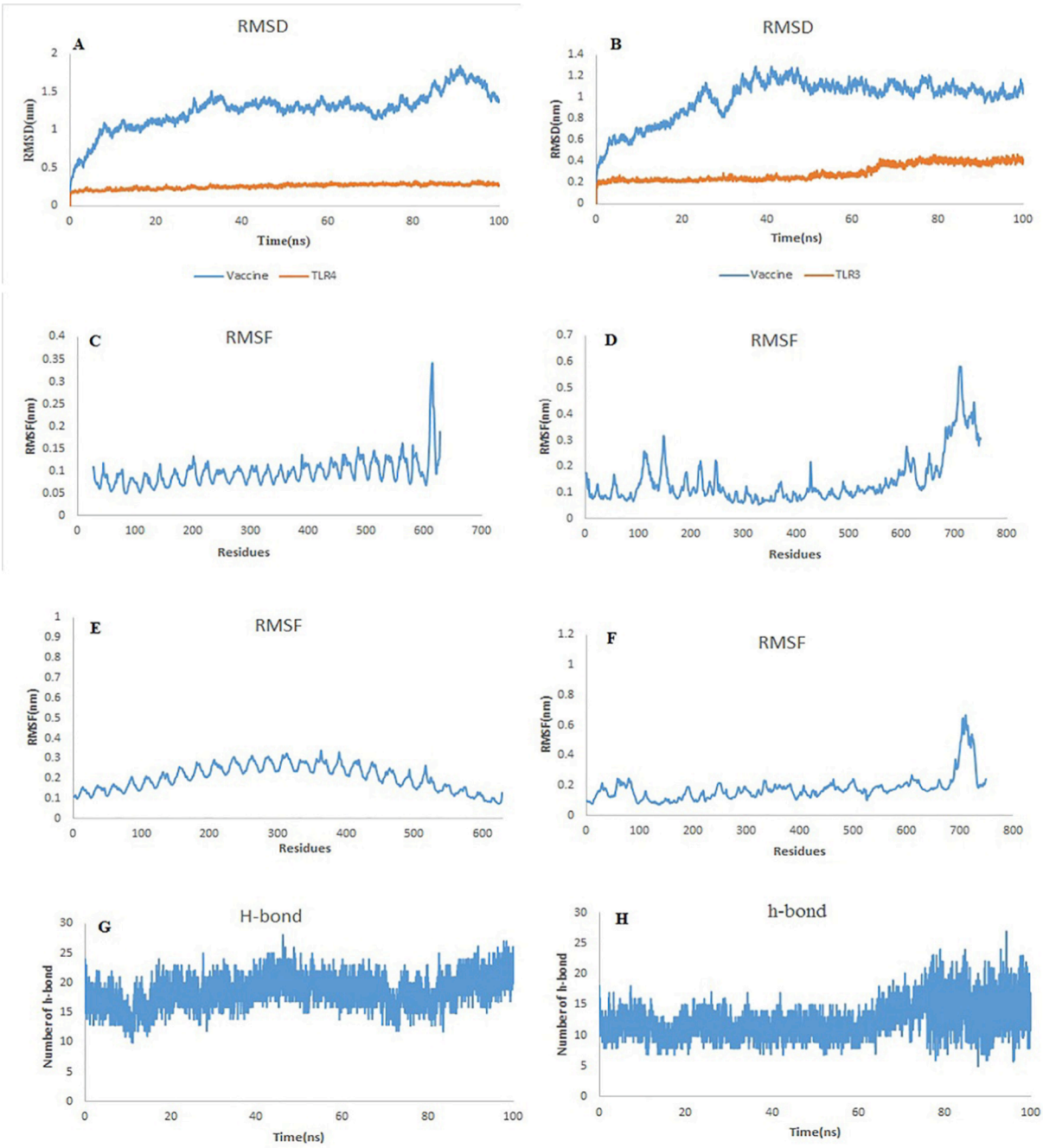

Fig. 12. MD simulation of the vaccine complex designed with TLR4 and TLR3. (A) An increasing trend has been observed in the RMSD plot for TLR4 and Vaccine since the simulation began. (B) An increasing trend has been observed in the RMSD plot for TLR3 and Vaccine since the simulation began. (C) Peaks represent regions of TLR4 with a high level of flexibility in the RMSF plot (D) RMSF plot in Vaccine (E) Peaks represent regions of TLR3 with a high level of flexibility in the RMSF plot (F) RMSF plot in Vaccine (G) Hydrogen bonds analysis between TLR4 and vaccine complex during MD simulations, (H) Hydrogen bonds analysis between TLR3 and vaccine complex during MD simulations.

its efficacy and safety. *E. coli* codon optimization was performed to achieve the maximum expression of the designed vaccine (strain K12). As a result, the CAI was 0.84, and the GC content was within an acceptable range at 50.17%, indicating a higher expression level in *E. coli* K-12. Multiple researchers have applied immunoinformatics to develop multi-epitope vaccine candidates [40,41,109]; epitope-based vaccines appear to activate immune cells, which may activate other immune cells via a complex signaling cascade [40,109].

Based on the discussion above, we believe the current study and similar multi-epitope vaccine design studies will improve the vaccination application against MPXV (and similar pathogens) and encourage extensive in vitro and in vivo research.

5. Conclusion

Following successive reports of monkeypox cases in the United Kingdom, United States, France, Spain, Brazil, and other countries in May 2022, the number of cases took a steady rise. However, few effective treatments or vaccines for MPXV are currently available on the market. This study aimed to investigate the immunoinformatics data of

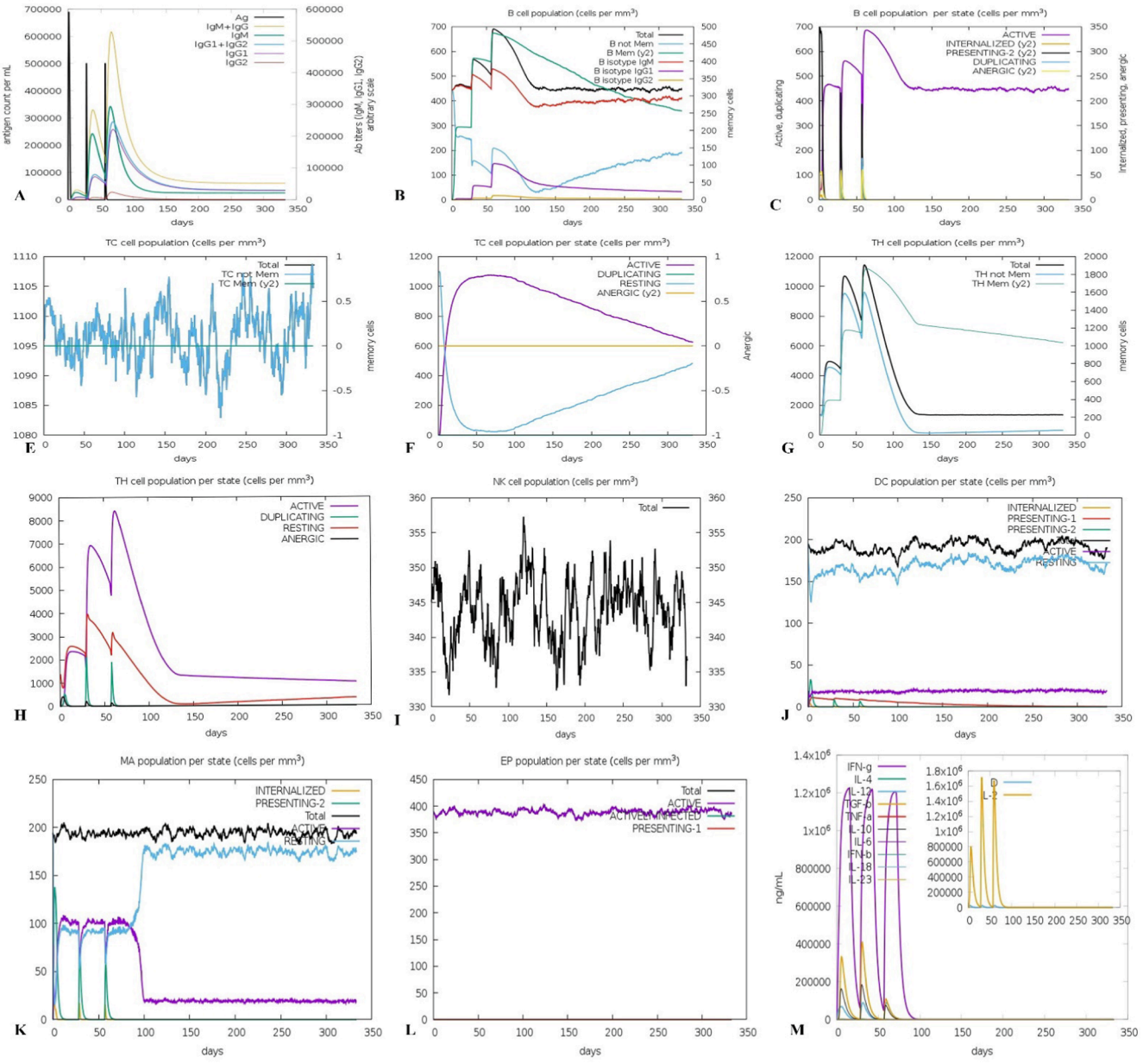

Fig. 13. The study observed contrasting outcomes between the in silico simulation and machine learning approaches when examining the immune response of humans following the administration of our MPXV vaccine construct. (A) The simulation indicates that the injection can increase immunoglobulin levels. The observed elevation of immunoglobulins varies depending on the concentration of the antigen, (B) The study reveals the presence of B lymphocytes (specifically IgM, IgG1, and IgG2) in the population after administering three doses of our vaccine construct (C) The figure illustrates the analysis results of the population per entity-state, representing different states such as active, presenting on class-II, internalized antigen, duplicating, and antigenic. Each state is depicted using a distinct color variant, (D) The data illustrates the changes in the population of cytotoxic T lymphocytes over a period of time (measured in days) following the administration of our MPXV vaccine formulation (E) The diagram depicts the population of Cytotoxic T lymphocytes in various conditions (resting and active) at different time intervals (days) following the administration of our MPXV vaccine design. (F) The diagram displays the overall count of TH cell population, including memory cells, categorized into different isotypes (IgM, IgG1, and IgG2) following the administration of our MPXV vaccine, (G) The figure demonstrates the count of Helper T cells categorized by entity-state, specifically the resting and active states, subsequent to the administration of our vaccine, (H) The behavior of the Population of Natural Killer cells. (I) The behavior of the population of Dendritic cells in the active and resting states after injection of our vaccine, (J) It shows the population of macrophages after MPXV vaccination, (K) Concentration of cytokines and interleukins with Simpson index [D], (L) The total number of EC cells is divided into three categories: active cells, virus-infected cells, and cells presenting on class-I MHC molecule. (Please refer to the Web version of this article for a better understanding of the color references mentioned in the figure legend).

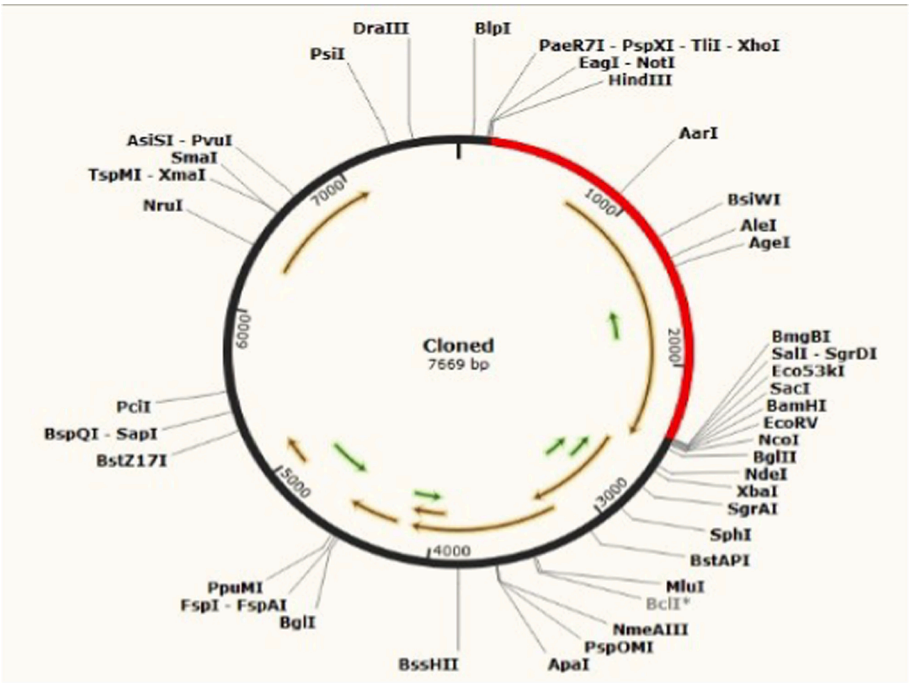

Fig. 14. In silico cloning of the vaccine construct. The pET-28 (+) backbone is shown in black and the vaccine construct is shown in red, surrounded between XhoI (158) and BamHI (1001).

A34L, A29L, B14R, E13L, and A27L proteins to identify effective and immunogenic B and T lymphocyte epitopes. After analyzing the sensitizing, toxicity, antigenic, and molecular binding properties, suitable links were used to connect the selected epitopes to the adjuvants, and the structure of the vaccine was formulated. Algorithms from the field of immunoinformatics predicted the secondary and tertiary structures of vaccines. Physical, chemical, and structural properties were refined and confirmed to achieve maximum stability. Molecular docking and molecular dynamics simulations were subsequently used to evaluate vaccine efficacy. After that, the ability of the vaccine to interact with toll-like receptors 3 and 4 (TLR3 and TLR4) was evaluated. Finally, the optimized sequence was then introduced into the Escherichia coli (E. coli) PET30A + vector. The predicted vaccine can theoretically be used against MPXV, and all these findings indicate that further research and development are needed to make it more effective. However, clinical studies and experimental validation are recommended to fully evaluate the efficacy of this multi-epitope vaccine.

Ethical approval

The Shahrekord University of Medical Sciences research ethics committee approved the study (IR.SKUMS.REC.1401.121).

Declaration of Competing Interest

The authors declare no conflict of interest.

Data availability

Data will be made available on request.

Acknowledgements

It is with great gratitude that the authors express their gratitude to the Shahrekord University of Medical Sciences (Shahrekord, Iran) for supporting this study.

Funding Sources

A grant number 6483 was awarded to this study by Shahrekord University of Medical Sciences.

References

[1] N. Kobayashi, Impact of Emerging, Re-Emerging and Zoonotic Viral Infectious Diseases, in a Virologist's Perspective, Open, Virol. J. 12 (2018) 131–133.
[2] K.T. Chen, Emerging Infectious Diseases and One Health: Implication for Public Health, Int. J. Environ. Res. Public Health 19 (15) (2022).
[3] J.P. Thornhill, S. Barkati, S. Walmsley, J. Rockstroh, A. Antinori, L.B. Harrison, R. Palich, A. Nori, I. Reeves, M.S. Habibi, Monkeypox virus infection in humans across 16 countries—April–June 2022, N. Engl. J. Med. 387 (8) (2022) 679–691.
[4] J.W. Jacobs, L. Filkins, G.S. Booth, B.D. Adkins, The potential impact of monkeypox infection and vaccination on blood donor deferrals and the blood supply, Br J Haematol. n/a(n/a) (2022).
[5] S. Aiman, Y. Alhamhoom, F. Ali, N. Rahman, L. Rastrelli, A. Khan, Q.u.A. Farooq, A. Ahmed, A. Khan, C. Li, Multi-epitope chimeric vaccine design against emerging Monkeypox virus via reverse vaccinology techniques- a bioinformatics and immunoinformatics approach, Front. Immunol. 13 (2022).
[6] H. Adler, S. Gould, P. Hine, L.B. Snell, W. Wong, C.F. Houlihan, J.C. Osborne, T. Rampling, M.B. Beadsworth, C.J. Duncan, J. Dunning, T.E. Fletcher, E. R. Hunter, M. Jacobs, S.H. Khoo, W. Newsholme, D. Porter, R.J. Porter, L. Ratcliffe, M.L. Schmid, M.G. Semple, A.J. Tunbridge, T. Wingfield, N.M. Price, Clinical features and management of human monkeypox: a retrospective observational study in the UK, Lancet Infect. Dis. 22 (8) (2022) 1153–1162.
[7] D.A. León-Figueroa, D.K. Bonilla-Aldana, M. Pachar, L. Romaní, H.M. Saldaña-Cumpa, C. Anchay-Zuloeta, M. Diaz-Torres, C. Franco-Paredes, J.A. Suárez, J. D. Ramirez, A. Paniz-Mondolfi, A.J. Rodriguez-Morales, The never-ending global emergence of viral zoonoses after COVID-19? The rising concern of monkeypox in Europe, North America and beyond, Travel Med Infect Dis 49 (2022), 102362.
[8] K. Simpson, D. Heymann, C.S. Brown, W.J. Edmunds, J. Elsgaard, P. Fine, H. Hochrein, N.A. Hoff, A. Green, C. Ihekweazu, T.C. Jones, S. Lule, J. Maclennan, A. McCollum, B. Mühlemann, E. Nightingale, D. Ogoina, A. Ogunleye, B. Petersen, J. Powell, O. Quantick, A.W. Rimoin, D. Ulaeato, A. Wapling, Human monkeypox - After 40 years, an unintended consequence of smallpox eradication, Vaccine 38 (33) (2020) 5077–5081.
[9] M.S. Mehand, F. Al-Shorbaji, P. Millett, B. Murgue, The WHO R&D Blueprint: 2018 review of emerging infectious diseases requiring urgent research and development efforts, Antiviral Res 159 (2018) 63-67.
[10] D. Kmiec, F. Kirchhoff, Monkeypox: A New Threat? Int. J. Mol. Sci. 23 (14) (2022).
[11] S.W. Shantier, M.I. Mustafa, A.H. Abdelmoneim, H.A. Fadl, S.G. Elbager, A. M. Makhawi, Novel multi epitope-based vaccine against monkeypox virus: vaccinomic approach, Sci. Rep. 12 (1) (2022) 15983.

[12] Y.-T. Lo, T.-W. Pai, W.-K. Wu, H.-T. Chang, Prediction of conformational epitopes with the use of a knowledge-based energy function and geometrically related neighboring residue characteristics, BMC Bioinf. 14 (4) (2013) S3.

[13] R.G. Swetha, S. Basu, S. Ramaiah, A. Anbarasu, Multi-Epitope Vaccine for Monkeypox Using Pan-Genome and Reverse Vaccinology Approaches, Viruses 14 (11) (2022).

[14] S. Sanami, S. Nazarian, S. Ahmad, E. Raeisi, M. Tahir Ul Qamar, S. Tahmasebian, H. Pazoki-Toroudi, M. Fazeli, M. Ghatreh Samani, In silico design and immunoinformatics analysis of a universal multi-epitope vaccine against monkeypox virus, PLoS One 18(5) (2023) e0286224.

[15] S.A.H. Abdi, A. Ali, S.F. Sayed, A. Abutahir, P.A. Ali, Multi-Epitope-Based Vaccine Candidate for Monkeypox: An In Silico Approach, Vaccines (Basel) 10 (9) (2022).

[16] M. Suleman, F. Rashid, S. Ali, H. Sher, S. Luo, L. Xie, Z. Xie, Immunoinformatic-based design of immune-boosting multiepitope subunit vaccines against monkeypox virus and validation through molecular dynamics and immune simulation, Front. Immunol. 13 (2022) 1042997.

[17] A. Ullah, F.A. Shahid, M.U. Haq, M. Tahir Ul Qamar, M. Irfan, B. Shaker, S. Ahmad, F. Alrumaihi, K.S. Allemailem, A. Almatroudi, An integrative reverse vaccinology, immunoinformatic, docking and simulation approaches towards designing of multi-epitopes based vaccine against monkeypox virus, J Biomol Struct Dyn (2022) 1-14.

[18] C. Hayat, M. Shahab, S.A. Khan, C. Liang, X. Duan, H. Khan, G. Zheng, Z. Ul-Haq, Design of a novel multiple epitope-based vaccine: an immunoinformatics approach to combat monkeypox, J. Biomol. Struct. Dyn. (2022) 1–12.

[19] N. Akhtar, V. Kaushik, R.K. Grewal, A.K. Wani, C. Suwattanasophon, K. Choowongkomon, R. Oliva, A.R. Shaikh, L. Cavallo, M. Chawla, Immunoinformatics-Aided Design of a Peptide Based Multiepitope Vaccine Targeting Glycoproteins and Membrane Proteins against Monkeypox Virus, Viruses 14 (11) (2022).

[20] K. Bhattacharya, I.M. Shamkh, M.S. Khan, M.M. Lotfy, J.B. Nzeyimana, R. F. Abutayeh, N.M. Hamdy, D. Hamza, N.R. Chanu, P. Khanal, A. Bhattacharjee, E. B. Basalious, Multi-Epitope Vaccine Design against Monkeypox Virus via Reverse Vaccinology Method Exploiting Immunoinformatic and Bioinformatic Approaches, Vaccines (Basel) 10 (12) (2022).

[21] S. Zaib, N. Rana, N. Areeba, H. Hussain, A.A. Alrbyawi, I. Dera, M. Khan, A. Khalid, A.-H. Khan, Designing multi-epitope monkeypox virus-specific vaccine using immunoinformatics approach, J. Infect. Public Health 16 (1) (2023) 107–116.

[22] M. Bhattacharya, S. Chatterjee, S. Nag, K. Dhama, C. Chakraborty, Designing, characterization, and immune stimulation of a novel multi-epitopic peptide-based potential vaccine candidate against monkeypox virus through screening its whole genome encoded proteins: An immunoinformatics approach, Travel Med. Infect. Dis. 50 (2022), 102481.

[23] M. Abrahim, A. Guterres, P.C. da Costa Neves, A.P.D. Ano Bom, The emergence of new lineages of the Monkeypox virus could affect the 2022 outbreak, bioRxiv (2022) 2022.07.07.498743.

[24] V. Franceschi, S. Parker, S. Jacca, R.W. Crump, K. Doronin, E. Hembrador, D. Pompilio, G. Tebaldi, R.D. Estep, S.W. Wong, M.R. Buller, G. Donofrio, BoHV-4-Based Vector Single Heterologous Antigen Delivery Protects STAT1(-/-) Mice from Monkeypoxvirus Lethal Challenge, PLoS Negl. Trop. Dis. 9 (6) (2015) e0003850.

[25] J.W. Hooper, D.M. Custer, E. Thompson, Four-gene-combination DNA vaccine protects mice against a lethal vaccinia virus challenge and elicits appropriate antibody responses in nonhuman primates, Virology 306 (1) (2003) 181–195.

[26] J.C. Ramírez, E. Tapia, M. Esteban, Administration to mice of a monoclonal antibody that neutralizes the intracellular mature virus form of vaccinia virus limits virus replication efficiently under prophylactic and therapeutic conditions, J. Gen. Virol. 83 (Pt 5) (2002) 1059–1067.

[27] R.D. Estep, I. Messaoudi, M.A. O'Connor, H. Li, J. Sprague, A. Barron, F. Engelmann, B. Yen, M.F. Powers, J.M. Jones, B.A. Robinson, B. U. Orzechowska, M. Manoharan, A. Legasse, S. Planer, J. Wilk, M.K. Axthelm, S. W. Wong, Deletion of the monkeypox virus inhibitor of complement enzymes locus impacts the adaptive immune response to monkeypox virus in a nonhuman primate model of infection, J. Virol. 85 (18) (2011) 9527–9542.

[28] J.C. Charity, E. Katz, B. Moss, Amino acid substitutions at multiple sites within the vaccinia virus D13 scaffold protein confer resistance to rifampicin, Virology 359 (1) (2007) 227–232.

[29] S.N. Shchelkunov, A.V. Totmenin, P.F. Safronov, M.V. Mikheev, V.V. Gutorov, O. I. Ryazankina, N.A. Petrov, I.V. Babkin, E.A. Uvarova, L.S. Sandakhchiev, J. R. Sisler, J.J. Esposito, I.K. Damon, P.B. Jahrling, B. Moss, Analysis of the monkeypox virus genome, Virology 297 (2) (2002) 172–194.

[30] I. Dimitrov, D.R. Flower, I. Doytchinova, AllerTOP - a server for in silico prediction of allergens, BMC Bioinf. 14 (6) (2013) S4.

[31] I.A. Doytchinova, D.R. Flower, VaxiJen: a server for prediction of protective antigens, tumour antigens and subunit vaccines, BMC Bioinf. 8 (2007) 4.

[32] C.S. Yu, C.W. Cheng, W.C. Su, K.C. Chang, S.W. Huang, J.K. Hwang, C.H. Lu, CELLO2GO: a web server for protein subCELlular LOcalization prediction with functional gene ontology annotation, PLoS One 9 (6) (2014) e99368.

[33] A. Krogh, B. Larsson, G. von Heijne, E.L. Sonnhammer, Predicting transmembrane protein topology with a hidden Markov model: application to complete genomes, J. Mol. Biol. 305 (3) (2001) 567–580.

[34] A. Garg, D. Gupta, VirulentPred: a SVM based prediction method for virulent proteins in bacterial pathogens, BMC Bioinf. 9 (1) (2008) 62.

[35] M.V. Larsen, C. Lundegaard, K. Lamberth, S. Buus, O. Lund, M. Nielsen, Large-scale validation of methods for cytotoxic T-lymphocyte epitope prediction, BMC Bioinf. 8 (2007) 424.

[36] B. Peters, S. Bulik, R. Tampe, P.M. Van Endert, H.G. Holzhütter, Identifying MHC class I epitopes by predicting the TAP transport efficiency of epitope precursors, J. Immunol. 171 (4) (2003) 1741–1749.

[37] M. Andreatta, M. Nielsen, Gapped sequence alignment using artificial neural networks: application to the MHC class I system, Bioinformatics 32 (4) (2016) 511–517.

[38] M. Nielsen, C. Lundegaard, P. Worning, S.L. Lauemøller, K. Lamberth, S. Buus, S. Brunak, O. Lund, Reliable prediction of T-cell epitopes using neural networks with novel sequence representations, Protein Sci. 12 (5) (2003) 1007–1017.

[39] K.K. Jensen, M. Andreatta, P. Marcatili, S. Buus, J.A. Greenbaum, Z. Yan, A. Sette, B. Peters, M. Nielsen, Improved methods for predicting peptide binding affinity to MHC class II molecules, Immunology 154 (3) (2018) 394–406.

[40] T. Kar, U. Narsaria, S. Basak, D. Deb, F. Castiglione, D.M. Mueller, A.P. Srivastava, A candidate multi-epitope vaccine against SARS-CoV-2. Sci Rep 10: 10895, Link: https://go.nature.com/3pUa0Mv (2020).

[41] L. Zhang, Multi-epitope vaccines: a promising strategy against tumors and viral infections, Cell. Mol. Immunol. 15 (2) (2018) 182–184.

[42] P. Wang, J. Sidney, C. Dow, B. Mothé, A. Sette, B. Peters, A systematic assessment of MHC class II peptide binding predictions and evaluation of a consensus approach, PLoS Comput. Biol. 4 (4) (2008) e1000048.

[43] J.J. Calis, M. Maybeno, J.A. Greenbaum, D. Weiskopf, A.D. De Silva, A. Sette, C. Keşmir, B. Peters, Properties of MHC class I presented peptides that enhance immunogenicity, PLoS Comput. Biol. 9 (10) (2013) e1003266.

[44] S.I. Islam, M.J. Mou, S. Sanjida, M. Tariq, S. Nasir, S. Mahfuj, Designing a novel mRNA vaccine against Vibrio harveyi infection in fish: an immunoinformatics approach, Genomics Inform 20 (1) (2022) e11.

[45] S.K. Dhanda, P. Vir, G.P. Raghava, Designing of interferon-gamma inducing MHC class-II binders, Biol. Direct 8 (2013) 30.

[46] S.K. Dhanda, S. Gupta, P. Vir, G.P.S. Raghava, Prediction of IL4 Inducing Peptides, Clin. Dev. Immunol. 2013 (2013), 263952.

[47] G. Nagpal, S.S. Usmani, S.K. Dhanda, H. Kaur, S. Singh, M. Sharma, G.P. Raghava, Computer-aided designing of immunosuppressive peptides based on IL-10 inducing potential, Sci. Rep. 7 (2017) 42851.

[48] S. Saha, G.P. Raghava, Prediction of continuous B-cell epitopes in an antigen using recurrent neural network, Proteins 65 (1) (2006) 40–48.

[49] M. Saadi, A. Karkhah, H.R. Nouri, Development of a multi-epitope peptide vaccine inducing robust T cell responses against brucellosis using immunoinformatics based approaches, Infect. Genet. Evol. 51 (2017) 227–234.

[50] M. Kavoosi, A.L. Creagh, D.G. Kilburn, C.A. Haynes, Strategy for selecting and characterizing linker peptides for CBM9-tagged fusion proteins expressed in Escherichia coli, Biotechnol. Bioeng. 98 (3) (2007) 599–610.

[51] D.D. Martinelli, In silico vaccine design: A tutorial in immunoinformatics, Healthcare Analytics 2 (2022), 100044.

[52] J. Kim, Y.L. Yang, Y. Jeong, Y.S. Jang, Application of Antimicrobial Peptide LL-37 as an Adjuvant for Middle East Respiratory Syndrome-Coronavirus Antigen Induces an Efficient Protective Immune Response Against Viral Infection After Intranasal Immunization, Immune Netw 22 (5) (2022) e41.

[53] E. Gasteiger, C. Hoogland, A. Gattiker, S.e. Duvaud, M.R. Wilkins, R.D. Appel, A. Bairoch, Protein Identification and Analysis Tools on the ExPASy Server, in: J. M. Walker (Ed.), The Proteomics Protocols Handbook, Humana Press, Totowa, NJ, 2005, pp. 571–607.

[54] I. Dimitrov, L. Naneva, I. Doytchinova, I. Bangov, AllergenFP: allergenicity prediction by descriptor fingerprints, Bioinformatics 30 (6) (2014) 846–851.

[55] M.W. Ng, G. Zhou, W.P. Chong, L.W.Y. Lee, H.K.W. Law, H. Zhang, W.H.S. Wong, S.F.S. Fok, Y. Zhai, R.W.H. Yung, E.Y. Chow, K.L. Au, E.Y.T. Chan, W. Lim, J.S. M. Peiris, F. He, Y.L. Lau, The association of RANTES polymorphism with severe acute respiratory syndrome in Hong Kong and Beijing Chinese, BMC Infect. Dis. 7 (1) (2007) 50.

[56] S.M.A. Hashemi, M. Thijssen, S.Y. Hosseini, A. Tabarraei, M.R. Pourkarim, J. Sarvari, Human gene polymorphisms and their possible impact on the clinical outcome of SARS-CoV-2 infection, Arch. Virol 166 (8) (2021) 2089–2108.

[57] D. Kovačić, A. Salihović, Multi-epitope mRNA Vaccine Design that Exploits Variola Virus and Monkeypox Virus Proteins for Elicitation of Long-lasting Humoral and Cellular Protection Against Severe Disease, Journal of, Med. Sci. (2022) e750.

[58] H.-H. Bui, J. Sidney, K. Dinh, S. Southwood, M.J. Newman, A. Sette, Predicting population coverage of T-cell epitope-based diagnostics and vaccines, BMC Bioinf. 7 (1) (2006) 153.

[59] L.J. McGuffin, K. Bryson, D.T. Jones, The PSIPRED protein structure prediction server, Bioinformatics 16 (4) (2000) 404–405.

[60] D.T. Jones, Protein secondary structure prediction based on position-specific scoring matrices, J. Mol. Biol. 292 (2) (1999) 195–202.

[61] C. Geourjon, G. Deleage, SOPMA: significant improvements in protein secondary structure prediction by consensus prediction from multiple alignments, Bioinformatics 11 (6) (1995) 681–684.

[62] J. Garnier, GOR secondary structure prediction method version IV, Meth. Enzym., RF Doolittle Ed. 266 (1998) 540-553.

[63] J. Yang, R. Yan, A. Roy, D. Xu, J. Poisson, Y. Zhang, The I-TASSER Suite: protein structure and function prediction, Nat. Methods 12 (1) (2015) 7–8.

[64] L. Heo, H. Park, C. Seok, GalaxyRefine: Protein structure refinement driven by side-chain repacking, Nucleic Acids Res. 41 (W1) (2013) W384–W388.

[65] R.A. Laskowski, J. Jabłońska, L. Pravda, R.S. Vařeková, J.M. Thornton, PDBsum: Structural summaries of PDB entries, Protein Sci. 27 (1) (2018) 129–134.

[66] C. Colovos, T.O. Yeates, Verification of protein structures: patterns of nonbonded atomic interactions, Protein Sci. 2 (9) (1993) 1511–1519.

[67] S.C. Lovell, I.W. Davis, W.B. Arendall Iii, P.I.W. De Bakker, J.M. Word, M. G. Prisant, J.S. Richardson, D.C. Richardson, Structure validation by Cα geometry: ϕ, ψ and Cβ deviation, Proteins Struct. Funct. Bioinf. 50 (3) (2003) 437–450.
[68] R.A. Laskowski, J.A.C. Rullmann, M.W. MacArthur, R. Kaptein, J.M. Thornton, AQUA and PROCHECK-NMR: programs for checking the quality of protein structures solved by NMR, J. Biomol. NMR 8 (4) (1996) 477–486.
[69] D. Kozakov, D. Beglov, T. Bohnuud, S.E. Mottarella, B. Xia, D.R. Hall, S. Vajda, How good is automated protein docking? Proteins 81 (12) (2013) 2159–2166.
[70] D. Kozakov, D.R. Hall, B. Xia, K.A. Porter, D. Padhorny, C. Yueh, D. Beglov, S. Vajda, The ClusPro web server for protein-protein docking, Nat. Protoc. 12 (2) (2017) 255–278.
[71] P.K. Raghav, R. Kumar, V. Kumar, G.P.S. Raghava, Docking-based approach for identification of mutations that disrupt binding between Bcl-2 and Bax proteins: Inducing apoptosis in cancer cells, Mol. Genet. Genomic Med. 7 (11) (2019) e910.
[72] P.K. Raghav, A. Raghav, A. Lathwal, A. Saxena, Z. Mann, M. Sengar, R. Rajalingam, Experimental and clinical data analysis for identification of COVID-19 resistant ACE2 mutations, Sci. Rep. 13 (1) (2023) 2351.
[73] J.X. Yang, J.C. Tseng, G.Y. Yu, Y. Luo, C.F. Huang, Y.R. Hong, T.H. Chuang, Recent Advances in the Development of Toll-like Receptor Agonist-Based Vaccine Adjuvants for Infectious Diseases, Pharmaceutics 14 (2) (2022).
[74] J.C. Flores-Canales, M. Kurnikova, Targeting Electrostatic Interactions in Accelerated Molecular Dynamics with Application to Protein Partial Unfolding, J. Chem. Theory Comput. 11 (6) (2015) 2550–2559.
[75] B. Hess, H. Bekker, 3 LINCS: a linear constraint solver for molecular simulations, J. Comp. Chem. 18 (1997) 1463–1472.
[76] P.K. Raghav, Y.K. Verma, G.U. Gangenahalli, Peptide screening to knockdown Bcl-2's anti-apoptotic activity: Implications in cancer treatment, Int. J. Biol. Macromol. 50 (3) (2012) 796–814.
[77] P.K. Raghav, Y.K. Verma, G.U. Gangenahalli, Molecular dynamics simulations of the Bcl-2 protein to predict the structure of its unordered flexible loop domain, J. Mol. Model. 18 (5) (2012) 1885–1906.
[78] A. Grote, K. Hiller, M. Scheer, R. Münch, B. Nörtemann, D.C. Hempel, D. Jahn, JCat: a novel tool to adapt codon usage of a target gene to its potential expression host, Nucleic Acids Res. 33 (Web Server issue) (2005) W526–W531.
[79] N. Rapin, O. Lund, M. Bernaschi, F. Castiglione, Computational Immunology Meets Bioinformatics: The Use of Prediction Tools for Molecular Binding in the Simulation of the Immune System, PLoS One 5 (4) (2010) e9862.
[80] F. Castiglione, F. Mantile, P. De Berardinis, A. Prisco, How the Interval between Prime and Boost Injection Affects the Immune Response in a Computational Model of the Immune System, Comput. Math. Methods Med. 2012 (2012), 842329.
[81] G.D. Gamage, A. Gunaratne, R.G. Periyannan, G.T. Russell, Applicability of Instability Index for In vitro Protein Stability Prediction, Protein Pept. Lett. 26 (5) (2019) 339–347.
[82] A. Roy, A. Kucukural, Y. Zhang, I-TASSER: a unified platform for automated protein structure and function prediction, Nat. Protoc. 5 (4) (2010) 725–738.
[83] H.X. Lim, J. Lim, S.D. Jazayeri, S. Poppema, C.L. Poh, Development of multi-epitope peptide-based vaccines against SARS-CoV-2, Biomed J. 44 (1) (2021) 18–30.
[84] S.W. Shantier, M.I. Mustafa, A.H. Abdelmoneim, H.A. Fadl, S.G. Elbager, A. M. Makhawi, Novel multi epitope-based vaccine against monkeypox virus: Vaccinomic approach, Sci. Rep. 12 (1) (2022) 1–17.
[85] M.R. Mauldin, A.M. McCollum, Y.J. Nakazawa, A. Mandra, E.R. Whitehouse, W. Davidson, H. Zhao, J. Gao, Y. Li, J. Doty, Exportation of monkeypox virus from the African continent, J Infect Dis 225 (8) (2022) 1367–1376.
[86] A. Vartak, S.J. Sucheck, Recent advances in subunit vaccine carriers, Vaccines 4 (2) (2016) 12.
[87] W.-Y. Zhou, Y. Shi, C. Wu, W.-J. Zhang, X.-H. Mao, G. Guo, H.-X. Li, Q.-M. Zou, Therapeutic efficacy of a multi-epitope vaccine against Helicobacter pylori infection in BALB/c mice model, Vaccine 27 (36) (2009) 5013–5019.
[88] M.H.V. Van Regenmortel, Mapping epitope structure and activity: from one-dimensional prediction to four-dimensional description of antigenic specificity, Methods 9 (3) (1996) 465–472.
[89] S. Shamriz, H. Ofoghi, N. Moazami, Effect of linker length and residues on the structure and stability of a fusion protein with malaria vaccine application, Comput. Biol. Med. 76 (2016) 24–29.
[90] F.R. Vogel, Improving vaccine performance with adjuvants, Clin. Infect. Dis. 30 (Supplement_3) (2000) S266–S270.
[91] B. Levast, S. Awate, L. Babiuk, G. Mutwiri, V. Gerdts, S. van Drunen Littel-van den Hurk, Vaccine potentiation by combination adjuvants, Vaccines 2 (2) (2014) 297–322.
[92] M.G. Netea, J.W.M. Van der Meer, R.P. Sutmuller, G.J. Adema, B.-J. Kullberg, From the Th1/Th2 paradigm towards a Toll-like receptor/T-helper bias, Antimicrob. Agents Chemother. 49 (10) (2005) 3991–3996.
[93] R. Arai, H. Ueda, A. Kitayama, N. Kamiya, T. Nagamune, Design of the linkers which effectively separate domains of a bifunctional fusion protein, Protein Eng. 14 (8) (2001) 529–532.
[94] M. Tahir ul Qamar, Z. Shokat, I. Muneer, U.A. Ashfaq, H. Javed, F. Anwar, A. Bari, B. Zahid, N. Saari, Multiepitope-based subunit vaccine design and evaluation against respiratory syncytial virus using reverse vaccinology approach, Vaccines 8 (2) (2020) 288.
[95] A. Mittal, S. Sasidharan, S. Raj, S.N. Balaji, P. Saudagar, Exploring the Zika genome to design a potential multiepitope vaccine using an immunoinformatics approach, Int. J. Pept. Res. Ther. 26 (4) (2020) 2231–2240.
[96] R. Ojha, N. Gupta, B. Naik, S. Singh, V.K. Verma, D. Prusty, V.K. Prajapati, High throughput and comprehensive approach to develop multiepitope vaccine against minacious COVID-19, Eur. J. Pharm. Sci. 151 (2020), 105375.
[97] J. Kim, Y.L. Yang, Y. Jeong, Y.-S. Jang, Application of Antimicrobial Peptide LL-37 as an Adjuvant for Middle East Respiratory Syndrome-Coronavirus Antigen Induces an Efficient Protective Immune Response Against Viral Infection After Intranasal Immunization, Immune Netw. 22 (5) (2022).
[98] B. Latimer, R. Toporovski, J. Yan, P. Pankhong, M.P. Morrow, A.S. Khan, N. Y. Sardesai, S.L. Welles, J.M. Jacobson, D.B. Weiner, Strong HCV NS3/4a, NS4b, NS5a, NS5b-specific cellular immune responses induced in Rhesus macaques by a novel HCV genotype 1a/1b consensus DNA vaccine, Hum. Vaccin. Immunother. 10 (8) (2014) 2357–2365.
[99] Y. Perrie, A.R. Mohammed, D.J. Kirby, S.E. McNeil, V.W. Bramwell, Vaccine adjuvant systems: enhancing the efficacy of sub-unit protein antigens, Int. J. Pharm. 364 (2) (2008) 272–280.
[100] M. Wiederstein, M.J. Sippl, ProSA-web: interactive web service for the recognition of errors in three-dimensional structures of proteins, Nucleic Acids Res. 35 (suppl_2) (2007) W407–W410.
[101] D.D. Chaplin, Overview of the immune response, J. Allergy Clin. Immunol. 125 (2) (2010) S3–S23.
[102] A. Boltjes, D. Movita, A. Boonstra, A.M. Woltman, The role of Kupffer cells in hepatitis B and hepatitis C virus infections, J. Hepatol. 61 (3) (2014) 660–671.
[103] W. Hu, Y.-T. Yen, S. Singh, C.-L. Kao, B.A. Wu-Hsieh, SARS-CoV regulates immune function-related gene expression in human monocytic cells, Viral Immunol. 25 (4) (2012) 277–288.
[104] A. Mubarak, W. Alturaiki, M.G. Hemida, Middle East respiratory syndrome coronavirus (MERS-CoV): infection, immunological response, and vaccine development, J. Immunol. Res. 2019 (2019).
[105] M. Shah, M.A. Anwar, J.-H. Kim, S. Choi, Advances in antiviral therapies targeting toll-like receptors, Expert Opin. Invest. Drugs 25 (4) (2016) 437–453.
[106] M. Yousaf, S. Ismail, A. Ullah, S. Bibi, Immuno-informatics profiling of monkeypox virus cell surface binding protein for designing a next generation multi-valent peptide-based vaccine, Front. Immunol. 13 (2022).
[107] S. Aziz, F.N. Almajhdi, M. Waqas, I. Ullah, M.A. Salim, N.A. Khan, A. Ali, Contriving multi-epitope vaccine ensemble for monkeypox disease using an immunoinformatics approach, Front. Immunol. 13 (2022).
[108] J. Thakar, M. Pilione, G. Kirimanjeswara, E.T. Harvill, R. Albert, Modeling systems-level regulation of host immune responses, PLoS Comput Biol. 3 (6) (2007) e109.
[109] M.A. Soltan, M.A. Eldeen, N. Elbassiouny, H.L. Kamel, K.M. Abdelraheem, H. A. El-Gayyed, A.M. Gouda, M.F. Sheha, E. Fayad, O.A.A. Ali, In silico designing of a multitope vaccine against rhizopus microsporus with potential activity against other mucormycosis causing fungi, Cells 10 (11) (2021) 3014.